



Spatial and temporal variability of the physical, carbonate and CO₂ properties in the Southern Ocean surface waters during austral summer (2005-2019)

Margaux Brandon, Catherine Goyet, Franck Touratier, Nathalie Lefèvre, Élodie Kestenare, Rosemary Morrow

► To cite this version:

Margaux Brandon, Catherine Goyet, Franck Touratier, Nathalie Lefèvre, Élodie Kestenare, et al.. Spatial and temporal variability of the physical, carbonate and CO₂ properties in the Southern Ocean surface waters during austral summer (2005-2019). Deep-sea research. Part A, Oceanographic research papers, 2022, 187, 10.1016/j.dsr.2022.103836 . insu-03778091

HAL Id: insu-03778091

<https://insu.hal.science/insu-03778091>

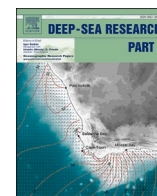
Submitted on 22 Sep 2022

HAL is a multi-disciplinary open access archive for the deposit and dissemination of scientific research documents, whether they are published or not. The documents may come from teaching and research institutions in France or abroad, or from public or private research centers.

L'archive ouverte pluridisciplinaire **HAL**, est destinée au dépôt et à la diffusion de documents scientifiques de niveau recherche, publiés ou non, émanant des établissements d'enseignement et de recherche français ou étrangers, des laboratoires publics ou privés.



Distributed under a Creative Commons Attribution - NonCommercial - NoDerivatives 4.0 International License



Spatial and temporal variability of the physical, carbonate and CO₂ properties in the Southern Ocean surface waters during austral summer (2005–2019)

Margaux Brandon^{a,*}, Catherine Goyet^b, Franck Touratier^b, Nathalie Lefèvre^a,
Elodie Kestenare^c, Rosemary Morrow^c

^a IRD-LOCEAN-IPSL, Sorbonne Université/CNRS/MNHN, 4 Place Jussieu, 75005, Paris, France

^b Laboratoire IMAGES-ESPACE-DEV, Univ. Perpignan Via Domitia, Perpignan, France

^c LEGOS, CNRS/IRD/CNES/University of Toulouse III, Toulouse, France

ARTICLE INFO

Keywords:

Southern ocean
Sea surface temperature and salinity
Carbonate system
Air-sea CO₂ flux
Spatial variability
Temporal variability

ABSTRACT

In situ measurements of sea surface temperature (SST), salinity (SSS), Total Alkalinity (A_T) and Total Carbon (C_T) were obtained during austral summer (mid-February to mid-March) from 2005 to 2019 in the Southern Ocean (SO), along a transect between Hobart, Tasmania and Dumont d'Urville French Antarctic Station. The studied transect is divided in four regions from North to South: the Subtropical Zone (STZ), the Subantarctic Region (SAR), the Antarctic Region (AAR) and the Coastal Antarctic Zone (CAZ). Latitudinal distribution of measured SST, SSS, A_T, C_T as well as calculated pH, CO₂ parameters (seawater fugacity of CO₂ (fCO_{2sw}), difference between seawater and atmospheric fCO₂ (ΔfCO₂), CO₂ flux (FCO₂)) and satellite-derived Chlorophyll *a* (Chl-*a*) are discussed. We show that the variability of physical and carbonate parameters in the STZ and north of the SAR are related to the mesoscale activity. In the CAZ, the freshwater inputs from sea-ice melting strongly impact the variability of all parameters. The comparison between physical and carbonate parameters highlights that A_T and C_T are directly related to the latitudinal variability of SST and SSS. Study of the CO₂ parameters shows that the transect is a sink of CO₂ during February and March, with a mean FCO₂ of $-4.0 \pm 2.8 \text{ mmol m}^{-2} \text{ d}^{-1}$. The most negative values of FCO₂ are found in the STZ and SAR north of 50°S and in the AAR south of 62°S, where biological activity is high. New simple empirical relationships are developed for A_T from SST and SSS and for C_T using SST, SSS and atmospheric fCO₂ (fCO_{2atm}) for the austral summer in the studied area. Using high resolution SSS and SST from the SURVOSTRAL program, trends of A_T and C_T are determined in the SAR and the AAR from 2005 to 2019. SST, SSS and A_T increase over this period in the SAR, which might be explained by the southward migration of the Subtropical Front. In the AAR, no clear trend is detected. C_T increases by 1.0 ± 0.2 and $0.8 \pm 0.3 \text{ } \mu\text{mol kg}^{-1} \text{ yr}^{-1}$ in the SAR and AAR respectively. The trend in the AAR is attributed to the increase in anthropogenic CO₂ emissions in the atmosphere while, in the SAR, hydrographic changes also contribute to the increase. Using the coefficient associated with fCO_{2atm} in the equation of C_T, we estimate the impact of atmospheric CO₂ increase on C_T at $1.18 \pm 0.14 \text{ } \mu\text{mol kg}^{-1} \text{ yr}^{-1}$ and $1.07 \pm 0.13 \text{ } \mu\text{mol kg}^{-1} \text{ yr}^{-1}$ in the SAR and AAR respectively. Decreases in pH are observed in both regions (-0.0018 ± 0.0001 and $-0.0026 \pm 0.0003 \text{ yr}^{-1}$ in the SAR and AAR respectively), indicating the sensitivity of surface waters in the area towards the development of ocean acidification processes under rising anthropogenic emissions.

1. Introduction

Since the pre-industrial period, the atmospheric CO₂ has increased rapidly due to increasing human activities. Up to a quarter of these anthropogenic CO₂ emissions have been absorbed by the global ocean

since then (Sabine et al., 2004; DeVries, 2014), with increasing uptake over the past decades (Gruber et al., 2019a, 2019b; Friedlingstein et al., 2020). But this uptake has consequences on the biogeochemistry of the ocean.

Over the past decades, increasing number of studies focused on the

* Corresponding author.

E-mail address: margaux.brandon@locean.ipsl.fr (M. Brandon).

<https://doi.org/10.1016/j.dsr.2022.103836>

Received 13 December 2021; Received in revised form 8 July 2022; Accepted 14 July 2022

Available online 19 July 2022

0967-0637/© 2022 The Authors. Published by Elsevier Ltd. This is an open access article under the CC BY-NC-ND license (<http://creativecommons.org/licenses/by-nc-nd/4.0/>).

changes in the physical, carbonate and CO₂ system to better constrain the impact of anthropogenic carbon (C_{ant}) on the global ocean. Under increasing atmospheric CO₂ concentration, C_T inventory has changed. Gruber et al. (2019a) estimated a total C_{ant} inventory of 34.4 PgC (petagrams of carbon) between 1994 and 2007 in the global ocean. In surface waters, C_T presents an increase around $1 \pm 0.6 \mu\text{mol kg}^{-1} \text{yr}^{-1}$ in different regions of the ocean (Bates et al., 2014; Takahashi et al., 2014; Lauvset et al., 2015; Merlivat et al., 2018; Lo Monaco et al., 2021; Gregor and Gruber, 2021), in part linked with the uptake of C_{ant}. In the intermediate and deep waters, storage of C_{ant} has also been observed, with strong spatial variability (Gruber et al., 2009, 2019a; Murata et al., 2010; Peng and Wanninkhof, 2010; Mahieu et al., 2020). As a consequence of the accumulation of C_{ant} in the ocean, pH has decreased by 0.1 since the beginning of the industrial era, leading to ocean acidification (Orr et al., 2005; Doney et al., 2009; Bates et al., 2014; Jiang et al., 2019).

The Southern Ocean (SO) is the key region in terms of C_{ant} uptake, accounting for 40% of the global ocean anthropogenic CO₂ absorption (Sabine et al., 2004; Mikaloff Fletcher et al., 2006; DeVries, 2014). At the surface, the waters unsaturated in CO₂ with respect to the atmosphere enhance the uptake of CO₂, while the intermediate and bottom-water formation in this region favours the export and storage of C_{ant} at depth (Gruber et al., 2009; DeVries, 2014). Moreover, the cold surface waters at high latitudes increase the solubility of CO₂, favouring the CO₂ uptake compared to warmer waters.

The understanding of the carbon cycle dynamics and the impact on the uptake of C_{ant} requires a good spatial and temporal coverage of in-situ data in the ocean, combining multiple parameters of the carbonate system, such as C_T, A_T, pH and CO₂ fluxes. Strong efforts have been made to increase these datasets, in particular measurements of surface waters fugacity of CO₂ (fCO_{2sw}), allowing us to quantify the CO₂ fluxes (FCO₂) between the ocean and the atmosphere. Most of these observations are based on spring and summer cruises. They have revealed a strong sink of CO₂ during summer in the SO, with mean FCO₂ around $-3 \text{ mmol m}^{-2} \text{d}^{-1}$ (Metzl et al., 1995; Brévière et al., 2006; Gray et al., 2018). The most important sinks are located in the Subantarctic Zone, Polar Front Zone and Seasonal Ice-free Zone during summer, with FCO₂ values down to $-20 \text{ mmol m}^{-2} \text{d}^{-1}$, and are associated with high biological activity in the surface waters (Metzl et al., 1999; Brévière et al., 2006; Gruber et al., 2009, 2019b; Gray et al., 2018). In contrast, the few studies available based on winter cruises or autonomous observation platforms have determined that this oceanic region was a source of CO₂ during winter, with FCO₂ values around $1 \text{ mmol m}^{-2} \text{d}^{-1}$ (Metzl et al., 1995, 1999, 2006; Gray et al., 2018). When focusing on longer time-scales, fCO_{2sw} observations show an increasing rate similar to that of the atmospheric fCO₂ (fCO_{2atm}) ($\sim 2 \mu\text{atm yr}^{-1}$) (Metzl, 2009; Takahashi et al., 2009; Munro et al., 2015; Lauvset et al., 2015; Xue et al., 2018; Leseurre et al., 2022), even as the CO₂ uptake by the SO has been fluctuating over the past decades (Le Quéré et al., 2007; Lovenduski et al., 2008; Lenton et al., 2013; Landschützer et al., 2015). The observed increase in C_{ant} in the SO drives the acidification of surface waters, with a decrease in pH quantified around $-0.002 \pm 0.001 \text{ yr}^{-1}$ (Midorikawa et al., 2012; Takahashi et al., 2014; Munro et al., 2015; Lauvset et al., 2015; Williams et al., 2015; Xue et al., 2018; Leseurre et al., 2022).

In the meantime, temperature and salinity observations are recording changes in heat content and oceanic circulation in the SO. Recent studies on the decadal evolution of temperature in the SO highlighted a warming of Subantarctic Surface and Intermediate Waters of around $0.2\text{--}0.3 \text{ }^{\circ}\text{C}$ per decade, while south of the Polar Front, the trend in SST is less clear, with small changes in the Antarctic Zone and a cooling of surface waters in the sea-ice zone in eastern Antarctica (Armour et al., 2016; Sallée, 2018; Auger et al., 2021). At the scale of the whole SO, SSS observations over past decades show different trends. While some studies present a freshening of surface waters (Durack and Wijffels 2010; Durack et al., 2012; de Laverne et al., 2014), others show no significant trend (Midorikawa et al., 2012; Takahashi et al., 2014;

Morrow and Kestenare, 2014). However, variations in westerly wind intensity, sea-ice concentration and gyre location have been observed in the past decades, with possible impact on the SSS as well as SST, and to a bigger scale, on SO circulation (Böning et al., 2008; de Laverne et al., 2014; Haumann et al., 2016; Morrow and Kestenare, 2017; Yang et al., 2020).

Despite the increasing amount of surface observations, data resolution is still sparse (Bakker et al., 2016; Gray et al., 2018). In particular, direct in situ measurements of A_T and C_T are scarce (Metzl et al., 2006; Laika et al., 2009; Midorikawa et al., 2012; Leseurre et al., 2022). The few estimated trends of A_T in the SO are often not significant or show important errors (Lenton et al., 2012; Midorikawa et al., 2012; Takahashi et al., 2014; Xue et al., 2018). On the opposite, all studies agree on an increase in C_T in all regions of the SO, with rates around $0.7 \pm 0.3 \mu\text{mol kg}^{-1} \text{yr}^{-1}$ (Lenton et al., 2012; Takahashi et al., 2014; Xue et al., 2018; Leseurre et al., 2022). This lack of observation limits the understanding of spatial distribution and temporal evolution of the carbonate system. Empirical relationships of A_T and C_T using SST and SSS are often used to complete the data coverage when no in situ measurements of the carbonate parameters are available (Lee et al., 2000, 2006). Previous studies have defined the equations of A_T and C_T in the SO, but these equations have been determined over the entire SO or are limited to a few cruises (Metzl et al., 1999; Lee et al., 2000, 2006; Laika et al., 2009).

Here we present the latitudinal distribution and decadal evolution of SST, SSS and carbonate parameters (A_T, C_T, pH, fCO_{2sw}, ΔfCO₂ - the difference between seawater and atmospheric fugacity, and FCO₂) along a transect south of Tasmania during austral summer (mid-February to mid-March) for the period 2005–2019. In order to complete our dataset, new simple empirical relationships of A_T and C_T are determined based on SSS and SST measurements and are compared with equations previously published in the SO. Temporal evolution of physical and carbonate parameters are investigated from 2005 to 2019. Finally, we discuss the impact of increasing C_{ant} uptake on the C_T inventory and on ocean acidification.

2. Material and methods

2.1. Data collection and satellite observations

In situ measurements of SST, SSS, A_T and C_T were obtained onboard RV *L'Astrolabe* between Hobart, Tasmania (43°S, 147°E) and Dumont d'Urville, Antarctica (67°S, 140°E) (Fig. 1) in austral summer (mid-February to mid-March) over the period 2005–2019 (Table 1). Continuous underway thermosalinograph measurements (SST, SSS) are part of the SURVOSTRAL program since 1993, and data used in this study cover the return trip during the entire period spanned by available A_T and C_T data between 2005 and 2019. Transects located too far away from the mean route were not considered. A total of 27 transects over 15 years were used for this study (<https://sss.sedoo.fr>, see Alory et al., 2015). These data were obtained at around 5 m depth every 1 min. The SSS accuracy is estimated to be between 0.005 and 0.01 (Morrow and Kestenare, 2014).

A_T and C_T were measured directly as part of the MINERVE program (<https://campagnes.flotteoceanographique.fr/series/128/fr/>), that aims to better understand the interannual variability of ocean-atmosphere CO₂ fluxes in the SO south of Tasmania. The data were collected between 2005 and 2019 but because of measurement accuracy issues, some transects were not used in this study, leading to a total of 9 cruises selected. For each A_T and C_T measurement, the closest SST and SSS measurements from SURVOSTRAL were chosen.

A_T and C_T were measured from surface waters (at 5 m depth) every 25 min for the cruises from 2005 to 2010 and every 2 h for 2019. Measurements were performed using a potentiometric method using a closed cell (Goyet et al., 1991). Until 2010, measurements were made using a fully automated system maintained at $18.0 \pm 0.1 \text{ }^{\circ}\text{C}$. The precision of A_T and C_T were estimated at 3.5 and $2.7 \mu\text{mol kg}^{-1}$,

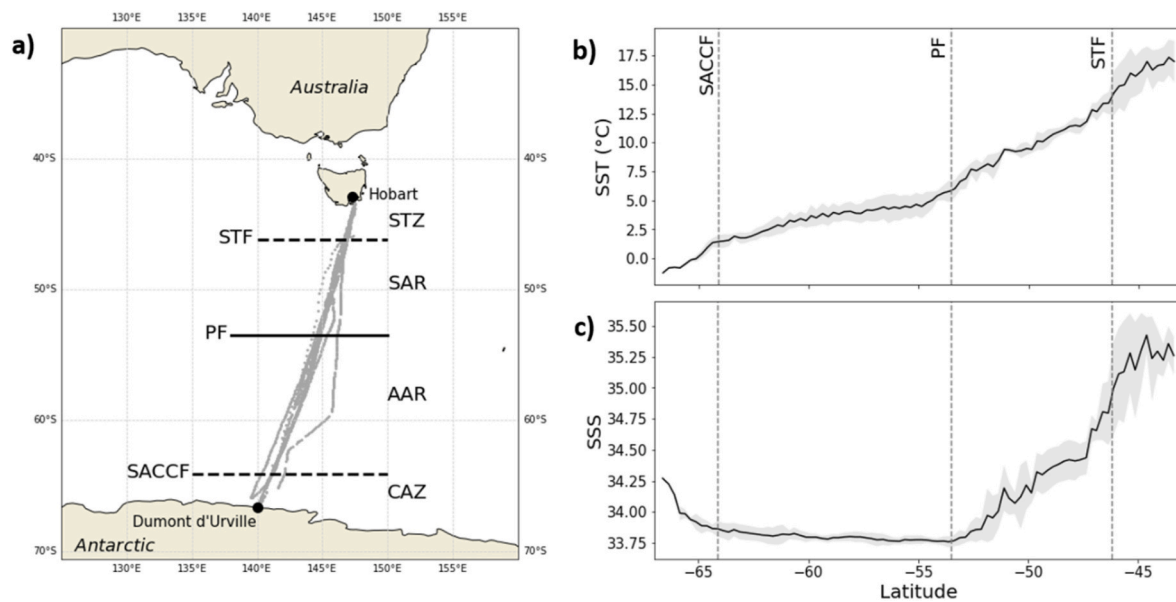


Fig. 1. a) Location of transects (grey lines) between Hobart, Tasmania and Dumont d'Urville, Antarctic. Oceanographic fronts and studied regions are located. STZ: Subtropical Zone, SAR: Subantarctic Region, AAR: Antarctic Region, CAZ: Coastal Antarctic Zone, STF: Subtropical Front, PF: Polar Front, SACC: Southern Antarctic Circumpolar Current Front. b) Latitudinal variation of Sea Surface Temperature (SST) and c) Salinity (SSS) from 2005 to 2019 collected at the same time as A_T and C_T . SST and SSS data have been averaged on 0.25° latitude bins. The black curve represents the mean value and the shaded grey area corresponds to one standard deviation.

Table 1

Cruises of the RV L'Astrolabe used in this study from the SURVOSTRAL program and availability of A_T and C_T measurements from the MINERVE program (HOB-DDU define data for the outward cruise and DDU-HOB for the return cruise).

year	Hobart-Dumont d'Urville	Dumont d'Urville-Hobart	Measured A_T and C_T
2005	18–23 Feb	26 Feb - 3 Mar	HOB-DDU, DDU-HOB
2006	17–22 Feb	25 Feb - 2 Mar	
2007	18–23 Feb	27 Feb - 4 Mar	DDU-HOB
2008	18–23 Feb	27 Feb - 2 Mar	HOB-DDU, DDU-HOB
2009	18–23 Feb	27 Feb - 4 Mar	DDU-HOB
2010	19–23 Feb	28 Feb - 5 Mar	HOB-DDU, DDU-HOB
2011	21–25 Feb	1–6 Mar	
2012		2–6 Mar	
2013	20–25 Feb	27 Feb - 4 Mar	
2014	1–6 Mar	12–16 Mar	
2015		14–18 Mar	
2016		1–5 Mar	
2017	23–28 Feb	2–7 Mar	
2018	20–24 Feb	28 Feb - 4 Mar	
2019	13–18 Feb	22–26 Feb	HOB-DDU

respectively. For 2019, discrete measurements were performed at IMAGES-ESPACE-DEV, Perpignan. The final dataset used for this study contains more than 188 000 measurements of in situ SST and SSS, and a total of 1755 observations of A_T , C_T .

Biological activity along the section was estimated for February and March of each year using 8-day composites of MODIS Aqua satellite images of Chlorophyll *a* (Chl-*a*) concentration at 4 km resolution, over the weeks covered by the cruises. Only data within a range of $\pm 3^\circ$ of longitude from the mean transect were selected and were zonally averaged for each available latitude.

2.2. Region determination and hydrographic fronts location

The SO is divided into multiple regions and zones, delimited by

hydrographic fronts (Orsi et al., 1995). These fronts are determined by strong temperature and salinity gradients. Based on the definitions of surface frontal signatures from Chaigneau and Morrow (2002), the dataset was divided in four regions: The Subtropical Zone (STZ), north of the Subtropical Front (STF); The Subantarctic Region (SAR), between the STF and the Polar Front (PF); the Antarctic Region (AAR), between the PF and the Southern Antarctic Circumpolar Current Front (SACC); and the Coastal Antarctic Zone (CAZ), south of the SACC down to the Antarctic coast (Fig. 1).

Using continuous SURVOSTRAL SST and SSS data for each cruise, we determined the mean position of each front along the transect. The STF is located around 46.2°S when SSS displays a strong gradient and SST shows a significant rapid decrease in latitude. The PF is defined as the northern limit of constant SSS of ~ 33.75 as well as a change in the slope of SST, its mean position is located along our sections at around 53.5°S . The position of the SACC is delimited by the decrease in SST and the increase in SSS at around 64.1°S . Within the SAR, the Subantarctic Front, defined with a gradient of SST and SSS around $49\text{--}52^\circ\text{S}$, divides the region into two zones, the Subantarctic Zone to the north and the Polar Front Zone to the south. This is the strongest subsurface front in the region and highly variable with strong mesoscale energy, yet on average, the mean surface characteristics of SST and SSS gradients are weaker (Fig. 1), so this front was not considered and the two zones were merged into the SAR. The same choice was made for the other weaker surface fronts associated with the Antarctic Circumpolar Current.

2.3. Determination of A_T and C_T from empirical relationships

In order to complete the dataset and have a better understanding of the long-term evolution of A_T and C_T , the carbonate parameters were calculated using relevant parameters affecting their variability.

The relationships were determined using TableCurve 3D software. Different equations forms (polynomial, logarithmic, exponential) were tested for the relationships. The simplest relationships with the best fit with measured data were chosen. Equations with associated coefficient and standard error are presented and are compared with existing ones in the Results and Discussion section.

2.4. Air-sea CO_2 flux

The $f\text{CO}_{2\text{sw}}$ was calculated with CO_2SYS software (Lewis and Wallace, 1998) for Python (Py CO_2SYS 1.6, Humphreys et al., 2022) using in situ measurements of SST, SSS, A_T and C_T as well as mean silicate and phosphate concentration for February and March of the World Ocean Atlas 2018 dataset (Garcia et al., 2019). Dissociation constants defined by Mehrbach et al. (1973) and refitted by Dickson and Millero (1987) as well as KHSO_4 dissociation constant from Dickson (1990) were used for the calculation. In order to complete the carbonate parameters, pH was also determined using Py CO_2SYS .

The $f\text{CO}_{2\text{atm}}$ was obtained from monthly $x\text{CO}_2$ measurements from Cape Grim, Tasmania (<https://gml.noaa.gov/dv/data/><https://www.csiro.au/greenhouse-gases/>), converted into $f\text{CO}_{2\text{atm}}$ at 100% humidity using monthly mean atmospheric pressure of the NCEP/NCAR

reanalysis project at $2.5^\circ \times 2.5^\circ$ grid and linearly interpolated at the position of each measurement along the transect (Data provided by the NOAA Physical Sciences Laboratory, Boulder, Colorado, USA, from their website at <https://psl.noaa.gov/data/gridded/data.ncep.reanalysis.html>).

The FCO_2 was calculated using the following approximate formula (neglecting the skin effect):

$$\text{FCO}_2 = k S_0 (f\text{CO}_{2\text{sw}} - f\text{CO}_{2\text{atm}}) \quad (1)$$

where S_0 the solubility of seawater CO_2 of Weiss (1974) and k , the gas transfer velocity, calculated using the formula of Wanninkhof (2014):

$$k = 0.251 U_{10}^2 \left(\frac{Sc}{660} \right)^{-0.5} \quad (2)$$

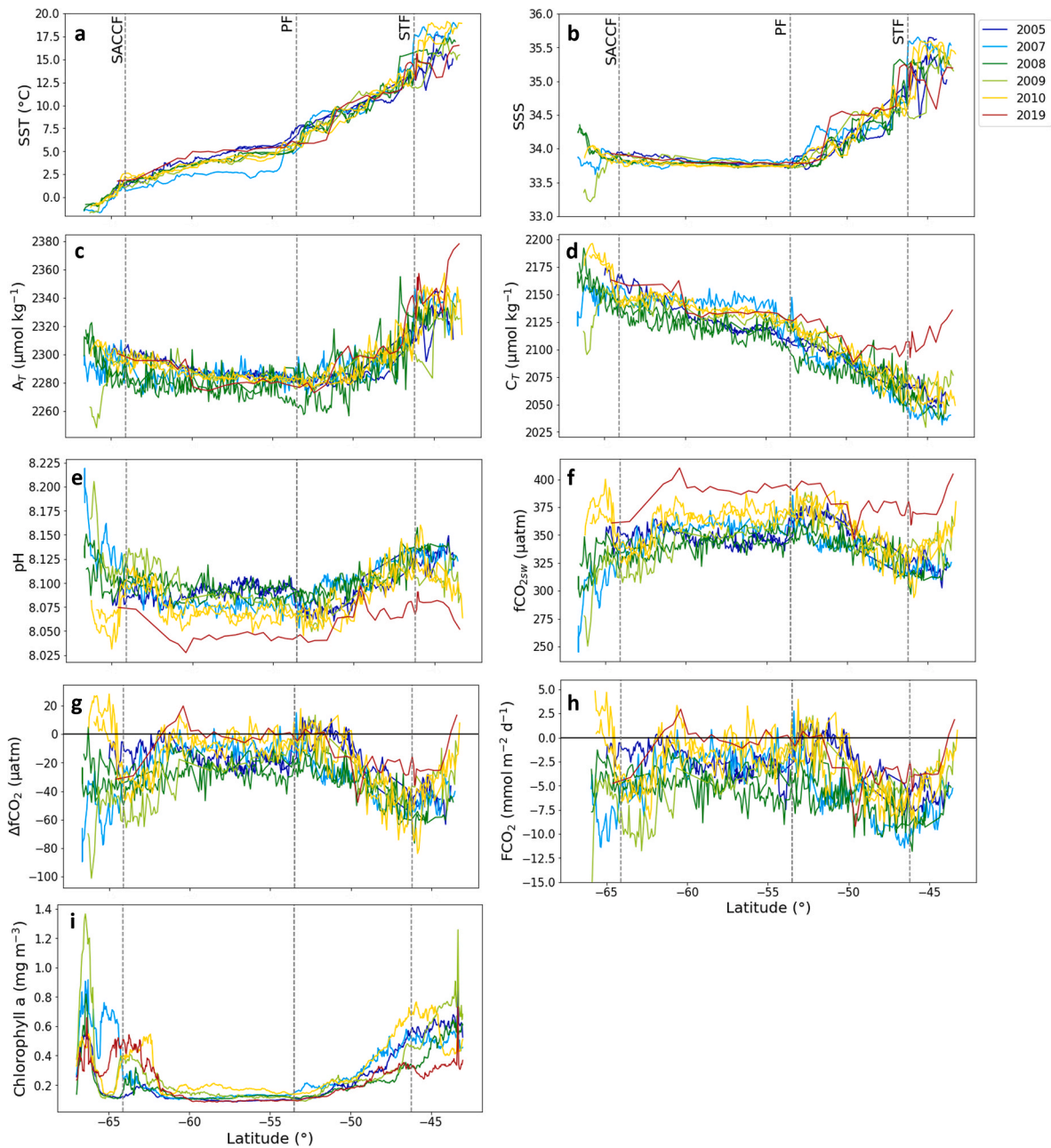


Fig. 2. Latitudinal variations of a) SST, b) SSS, c) A_T , d) C_T , e) pH, f) calculated $f\text{CO}_{2\text{sw}}$, g) $\Delta f\text{CO}_2$, h) FCO_2 and i) MODIS Aqua satellite observation of mean Chl-a for February and March between 2005 and 2019, for the years when A_T and C_T measurements are available. Dotted lines indicate the location of the fronts, from north to south: Subtropical Front (STF), Polar Front (PF) and Southern Antarctic Circumpolar Current Front (SACCF).

where U_{10} is the wind speed at 10 m above sea level and Sc , the Schmidt number.

The monthly mean wind speed was taken from the Remote Sensing Systems website (Wentz et al., 2015; <https://remss.com/measurements/wind/>) and was co-located at each measurement location.

3. Results and Discussion

3.1. Latitudinal distribution of surface physical, carbonate and CO_2 parameters between Hobart and Dumont d'Urville

We first present the latitudinal distribution of physical (SST, SSS), carbonate (A_T , C_T , pH) and CO_2 parameters (fCO_{2sw} , ΔfCO_2 - the difference between seawater and atmospheric fCO_2 , and fCO_2) as well as Chl-a satellite data along the transect for the period 2005–2019. We also discuss the relation between measured physical and carbonate parameters.

3.1.1. SST and SSS

SST shows a southward decrease from 16.12 ± 1.89 °C in the STZ to -0.10 ± 1.06 °C in the CAZ (Fig. 2a). As described in the methodology section, SST presents strong gradients at the position of hydrographical fronts, leading to a non-linear cooling of surface waters along the transect. During the 2007 cruise, mean SST in the AAR is 1.41 °C cooler than the mean of other years. South of Tasmania, the fronts associated with the ACC are constrained by the Southeast Indian Ridge topography and form a quasi-permanent meander extending northward at around 145°E that brings colder waters up to 55°S of latitude (Sokolov and Rintoul, 2002; Park et al., 2019). The observed SST anomaly during 2007 can be explained by the eastward location of the cruise compared to all other cruises, and therefore crossing the meander formed with colder waters, highlighting the strong spatial variability of the fronts. SSS also shows a southward decrease from 35.27 ± 0.29 in the STZ to a value of 33.78 ± 0.05 at the PF (Fig. 2b). Surface waters in the STZ and the northern part of the SAR along the transect are influenced by the southward transport of subtropical warm and salty waters, originating from the Tasman Sea and carried by the East Australian Current (EAC) and Tasman Outflow to the East and by the Zeehan Current (ZC) to the West (Cresswell, 2000; Ridgway, 2007; Herraiz-Borreguero and Rintoul, 2010, 2011; Morrow and Kestenare, 2014; Pardo et al., 2017). Both SST and SSS present strong mesoscale and interannual variability in the STZ and also in the SAR. This variability can originate from two mechanisms. First, variations in the strength of the ZC and the EAC have been linked to large-scale changes in wind stress that impact on the southward transport of subtropical waters (Cai et al., 2005; Oliver et al., 2016; Oliver and Holbrook, 2018). The other mechanism that contributes to this variability is the presence of energetic mesoscale eddies and meanders along the STF and SAF (Chaigneau et al., 2004; Sokolov and Rintoul, 2009; Herraiz-Borreguero and Rintoul, 2011; Morrow and Kestenare, 2014). Previous studies in the region also highlighted the presence of cold-cores or cyclonic eddies originating from a meander (Morrow et al., 2004; Moreau et al., 2017). In our case, the local drops in SST and SSS observed in the STZ during 2005 and 2019 cruises could be explained by the northward migration of a cyclonic eddies formed south of the SAF.

In the AAR, the salinity is quite stable, showing only a 0.09 ± 0.05 increase from north to south of the region, with little variability. As described by Chaigneau and Morrow (2002) and Chaigneau et al. (2004), the layer of near-constant salinity at the surface of this region can be explained by strong Ekman and geostrophic currents, that transport freshwater from sea-ice melt in a north-eastward direction during spring and summer.

Finally, in the CAZ, SST rapidly decreases towards negative values whereas SSS shows strong variability, with values ranging between 33.21 and 34.35. While SSS drops drastically to 33.62 and 33.21 during the 2007 and 2009 cruises, respectively, we observe an increase in SSS in

2008. The SSS close to the coasts of Antarctica is strongly influenced by the formation and melting of sea-ice through the year and the lateral advection of sea-ice along the coast (Morrow and Kestenare, 2017). The peak in freshwaters recorded during summer in the CAZ are the consequence of late sea-ice melting, while the increase in SSS observed in 2008 may reflect less sea-ice and the presence of saltier shelf waters near the coast of Antarctica, or early sea-ice formation during late summer linked with brine rejection (Chaigneau and Morrow, 2002). The annual SSS measurements from SURVOSTRAL over 2005–2019 clearly shows the strong interannual variability depending on sea-ice melting and formation (Supplementary Fig. 1).

3.1.2. Carbonate parameters (A_T , C_T , pH)

The highest A_T values (mean $2331.2 \mu\text{mol kg}^{-1}$) are recorded in the STZ before decreasing along the transect to reach a mean of $2279.4 \pm 8.3 \mu\text{mol kg}^{-1}$ at the PF (Fig. 2c). In the AAR, A_T slightly increase southward from 2279.8 ± 6.8 to $2293.1 \pm 8.7 \mu\text{mol kg}^{-1}$. In the CAZ, A_T shows strong variability, with mean value of $2294.4 \pm 12.6 \mu\text{mol kg}^{-1}$ and a minimum of $2248.0 \mu\text{mol kg}^{-1}$ in 2009. Through the transect, A_T latitudinal distribution strongly resembles that of SSS, emphasizing that A_T variability is governed by the same factors impacting salinity (Fig. 3b). Indeed, In the surface ocean, A_T is dependent on salinity changes through freshwater inputs and removal (precipitation-evaporation, sea-ice melting-formation), contributing to more than 80% of A_T variability (Millero et al., 1998; Fry et al., 2015). However, when looking at the SSS- A_T diagram (Fig. 3b), a linear relationship is only observed north of the PF and during episodes of freshening of surface waters in the CAZ. South of the PF, A_T is inversely related to changes in SST (Fig. 3a). This relationship can be explained by the presence of upwelling of cold and A_T -rich waters in the high latitudes of the SO (Millero et al., 1998; Key et al., 2004; Fry et al., 2015; Fine et al., 2017). The only exception to the SST- A_T relationship south of the PF is in the CAZ, when strong freshening of surface waters impact A_T , while SST does not register any major change. In the STZ and SAR, the strong variability observed in the physical parameters seems to have a moderate impact on A_T . However, some intense events such as the rapid drop in SST and SSS at 45°S during 2005 cruise, lead to strong variability in A_T - in this case, a decrease in A_T of around $25 \mu\text{mol kg}^{-1}$. This highlights the importance of both SSS and SST in the variability of A_T .

C_T presents a mean southward increase from $2058.9 \pm 13.9 \mu\text{mol kg}^{-1}$ in the STZ to $2156.3 \pm 19.4 \mu\text{mol kg}^{-1}$ in the CAZ (Fig. 2d). However, the rise in C_T is not linear and changes of slope can be observed at the position of the fronts. The latitudinal distribution of C_T is inversely related to the one of SST, as shown by the linear negative relationship observed on the SST- C_T diagram (Fig. 3c). The poleward rise observed in C_T concentration is influenced by the decrease in SST, leading to an increase in solubility of CO_2 at the ocean surface, but also, to a smaller extent, by the upwelling of C_T -rich waters south of the Polar Front (Wu et al., 2019 and references therein). Like A_T , no relationship is observed between SSS and C_T south of the PF (Fig. 3d). North of the PF, however, a negative relationship is observed between both parameters. During episodes of surface waters freshening in the CAZ, C_T is also affected by the decrease in SSS. Because the SST is only slightly affected by these events, we observe no clear relationship between SST and C_T during these events, as seen for A_T .

Besides changes in solubility and evaporation/precipitation, surface C_T is also influenced by biological processes (primary production, calcification). Increase in biological activity at the surface ocean would decrease the C_T , as seen off the South-East coast of Madagascar in 2020 (Metzl et al., 2022). Along the studied transect, satellite images show higher Chl-a concentration north of 51°S and south of 62°S (Fig. 2i). However, the concentrations stay quite low and no clear decrease in C_T are observed at the same locations.

Finally, surface C_T is also modulated by the difference in fCO_2 between the atmosphere and the surface ocean. Because of the increase in anthropogenic emissions, variations in C_T are not only from natural

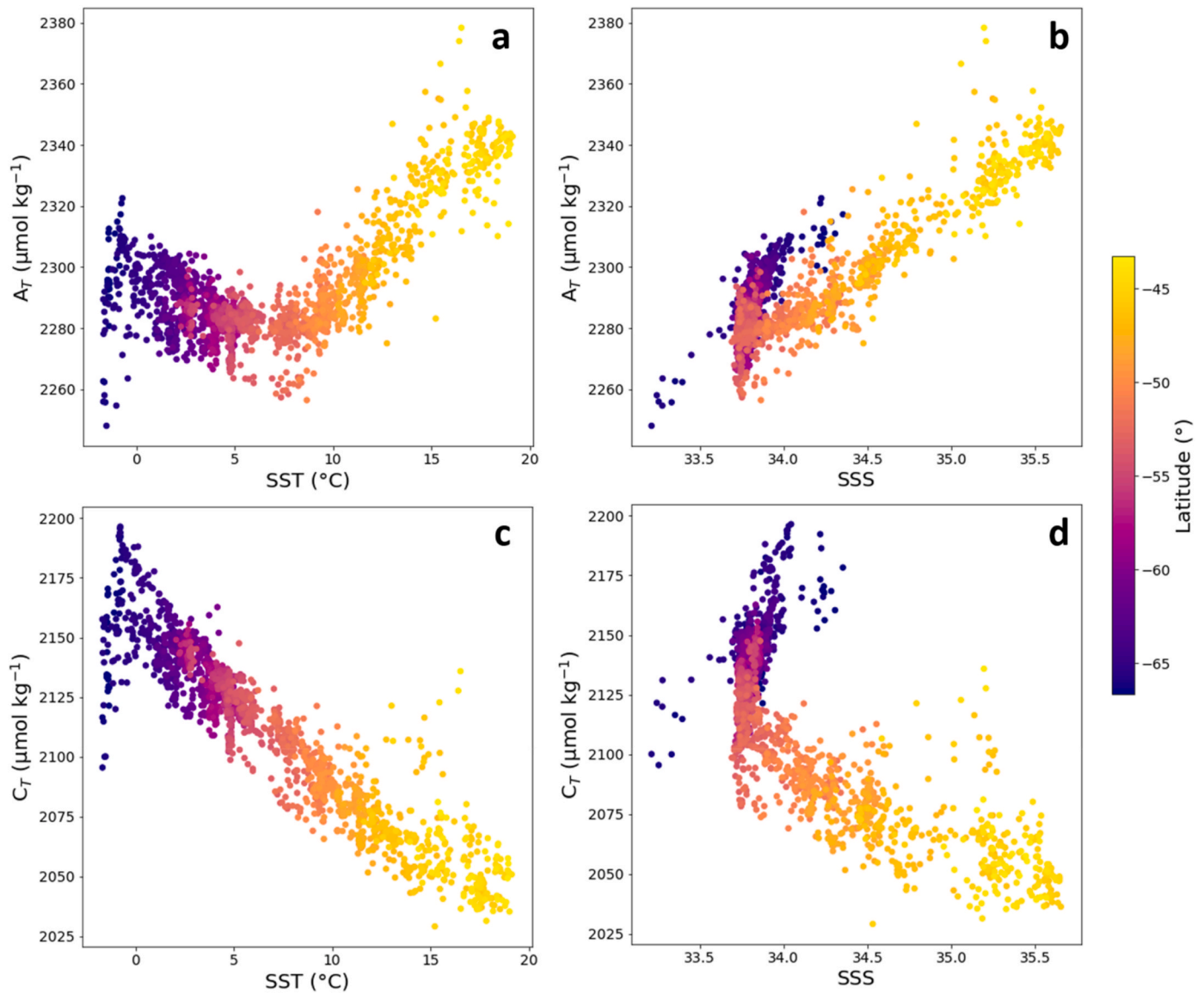


Fig. 3. Relationship between physical and carbonate parameters depending on latitude along the Hobart-Dumont d'Urville transect. a) SST- A_T , b) SSS- A_T , c) SST- C_T , d) SSS- C_T .

origin but also from anthropogenic origin (C_{ant}). While C_T can be measured in-situ, C_{ant} cannot be measured directly. Multiple approaches using carbonate system parameters have been carried out over these past decades to quantify the uptake and storage of C_{ant} by the ocean below the surface and to identify the oceanic regions of importance for the sink of CO_2 and C_{ant} (Chen, 1982, 1993; Coatanoan et al., 2001; Gruber et al., 2009; Sabine and Tanhua, 2010 and references therein). But because of the complexity of the spatial and temporal variability of physical and biological processes occurring in the surface layer, the part of surface C_T from anthropogenic origin is difficult to differentiate from C_T of natural origin. The evolution of C_T in a context of increasing anthropogenic emission will be discussed in the last chapter.

In 2019, higher C_T is observed in the STZ and north of the SAR, with a mean value of $40.3 \pm 3.8 \mu\text{mol kg}^{-1}$ higher compared to the mean of cruises between 2005 and 2010. Several factors could explain this major shift in C_T concentration. First, surface waters are affected by the increasing uptake of C_{ant} . In particular, subtropical and subantarctic waters have high anthropogenic CO_2 concentrations (Sabine et al., 2004; Carroll et al., 2022), and over the past decades, an accumulation of C_{ant} in the upper water-column has been registered north of 50°S along a

transect close to this study (Carter et al., 2019). A part of the increase in C_T observed in 2019 could therefore originate from rising C_{ant} in surface waters. Then, because of the strong mesoscale activity in this region, a part of this increase could also be related to the presence of a cyclonic eddy along the cruise transect. Indeed, Moreau et al. (2017) showed that the inner surface waters had higher C_T concentrations compared to waters outside the eddy. Finally, lower biological activity could also act to increase the mean surface C_T concentrations in this region, as seen in Fig. 2i.

Surface pH, calculated using measured physical and carbonate parameters, ranges between 8.028 and 8.219 (Fig. 2e). The highest values are located around the STF and in the CAZ. Strong variability in pH is observed in this latter zone, with a maximum difference of 0.188. 2019 values are clearly lower than during years 2005–2019. This trend will be further discussed in the last section of the discussion.

3.1.3. Air-sea CO_2 exchanges and biological activity

fCO_{2sw} ranges between 245.0 and $410.1 \mu\text{atm}$ and the latitudinal distribution shows strong variability (Fig. 2f). The highest mean values are located at the northern and southern limit of the transect and

between 51°S and 62°S, while waters around the STF (between 44 and 51°S) and in the AAR south of 62°S present values down to 300 μatm . In the CAZ, $f\text{CO}_{2\text{sw}}$ presents a strong variability, with values between 245.0 and 400.1 μatm . Besides the spatial variability, changes in $f\text{CO}_{2\text{sw}}$ can be observed at the temporal scale for a same location. The most striking pattern is the mean increase of 34.6 μatm in $f\text{CO}_{2\text{sw}}$ in the 2019 cruise compared to the period 2005–2010. A concomitant increase of 28.8 μatm is measured in the $f\text{CO}_{2\text{atm}}$ between 2005 and 2019, originating from the rise in atmospheric CO_2 throughout years. The highest mean increase in $f\text{CO}_{2\text{sw}}$ compared to the atmosphere could originate from the interannual variability in ocean dynamics and/or biological activity. When considering the change in $f\text{CO}_{2\text{sw}}$ with respect to $f\text{CO}_{2\text{atm}}$, the $\Delta f\text{CO}_2$ values during 2019 are closer to the ones of the years 2005–2010, highlighting that the equilibrium between atmosphere and ocean have not changed much. Mean $\Delta f\text{CO}_2$ and FCO_2 values range from $-56.5 \mu\text{atm}$ to $-4.0 \mu\text{atm}$ and from $-8.0 \text{ mmol m}^{-2} \text{ d}^{-1}$ to $-0.3 \text{ mmol m}^{-2} \text{ d}^{-1}$ respectively along the transect, and present similar trends to $f\text{CO}_{2\text{sw}}$ (Fig. 2g and 2). Around the STF and in the AAR south of 62°S, the surface waters are undersaturated with respect to the atmosphere, with mean values of $\Delta f\text{CO}_2$ and FCO_2 down to $-52.0 \mu\text{atm}$ and $-35.2 \text{ mmol m}^{-2} \text{ d}^{-1}$ respectively, defining these regions as strong sink of CO_2 . The areas close to Tasmania coast and between 51 and 62°S show a reduced uptake in CO_2 , with punctual $\Delta f\text{CO}_2$ higher than 0, located in the southern part of the SAR and at 61°S. The studied region is therefore a sink of CO_2 during the end of summer, with a mean FCO_2 of $-4.0 \pm 2.8 \text{ mmol m}^{-2} \text{ d}^{-1}$. The spatial distribution in air-sea exchanges in CO_2 have been previously observed in the region south of Tasmania over the same period of the year, with direct measurements of $f\text{CO}_2$ (Metzl et al., 1999; Brévière et al., 2006; Laika et al., 2009; Benallal et al., 2017). These studies all showed sinks of CO_2 north of 50°S approximately, with minimum values between 300 and 320 μatm , and $\Delta f\text{CO}_2$ down to $-60 \mu\text{atm}$. In the southern part of the SAR and northern part of the AAR, they found a smaller sink or a small source, with $\Delta f\text{CO}_2$ around 0 μatm (Brévière et al., 2006; Laika et al., 2009). In summer 2003, Brévière et al. (2006) found low $\Delta f\text{CO}_2$ (around $-40 \mu\text{atm}$), but this strong sink was concomitant with unusually strong biological activity in the area, as revealed by Chl-a concentration from satellite images. Finally, in the southern part of the AAR and in the CAZ, Laika et al. (2009) and Benallal et al. (2017) found a sink of CO_2 with $\Delta f\text{CO}_2$ around $-40 \mu\text{atm}$ and FCO_2 around $-4.0 \pm 2.0 \text{ mmol m}^{-2} \text{ d}^{-1}$. The comparison of our dataset ($f\text{CO}_{2\text{sw}}$, $\Delta f\text{CO}_2$ and FCO_2) with the measured ones in the literature showed a very good agreement, confirming the validity of our calculated values of $f\text{CO}_{2\text{sw}}$ and FCO_2 .

The strong sinks in CO_2 north of 51°S and in the AAR south of 62°S coincide with higher values of Chl-a along the transect (Fig. 2i). Satellite images of Chl-a concentrations over the weeks covered by cruises show values between 0.08 and 1.36 mg m^{-3} . The surface waters between 51 and 62°S are almost free of Chl-a, while north of 51°S and south of 62°S, mean weekly Chl-a values reach values up to 1 mg m^{-3} , still with a strong spatial and temporal variability within these areas. In the SO south of Tasmania, high biological activity is observed from austral spring to the end of austral summer, with strong phytoplankton blooms north of 50°S and south of 60°S, caused by the development of lightly silicified diatoms and coccolithophores in the north and highly silicified diatoms in the south (Balch et al., 2016; Nissen et al., 2021). Despite the difference in temporal and spatial resolution between CO_2 fluxes from in-situ data and Chl-a concentrations from 8-day composite satellite images, the observed decreases in FCO_2 towards more negative values seem to be strongly controlled by higher biological activity along the transect. Similar undersaturation of surface waters have been observed in a context of high Chl-a concentration in the SO in previous studies, confirming the direct influence of biological activity on the presence of sinks of CO_2 (Brévière et al., 2006; Laurantou and Metzl, 2011).

3.2. Processes affecting the variability of A_T and C_T

3.2.1. Drivers of A_T variability

As previously seen, in the SO south of Tasmania, we observe a relationship between A_T and SSS in the surface waters north of the PF. In the AAR however, A_T is more related to changes in SST. Both parameters are therefore useful to calculate A_T along the studied transect. Here, we determine an empirical relationship for A_T using measured SSS and SST along the transect. Because most of the measurements stop before Dumont d'Urville Station, the data available in the CAZ are not sufficient to evaluate a robust relation between the parameters as well as their temporal variability. Data in the STZ are not considered either, because of the influence of the Tasmanian Coast and of the strong spatial variability of the data in the STZ. The dataset is therefore composed of a total of 1413 samples over 6 different years from 2005 to 2019 and located in the SAR and AAR.

We determined a linear dependence between A_T and SSS and SST, resulting the following equation:

$$A_{T_{\text{calc}}} = 762.69 (\pm 37.03) + 45.28 (\pm 1.11) * \text{SSS} - 2.15 (\pm 0.10) * \text{SST} \quad (3)$$

Coefficients are presented in Table 2. The difference between measured A_T and calculated A_T using Equ. 3, ΔA_T , is $-0.02 \mu\text{mol kg}^{-1}$ with a root mean squared error (RMSE) of $6.71 \mu\text{mol kg}^{-1}$. The simplest relationships were chosen as more complex ones did not significantly improved the fit. No major difference was observed between the calculation of A_T for the two regions individually or together. Therefore, a unique equation for the area combining SAR and AAR was selected (Equation (3) and Table 2).

Empirical relationships have been previously developed to calculate A_T from physical parameters in the SO, some of them being valid for the whole SO (Lee et al., 2006) while others being valid for a specific region of the SO (Metzl et al., 1999; Laika et al., 2009; Shadwick et al., 2015) (Table 3). When using these equations, considerations should also be taken on the period of time covered by the dataset used to develop the relationship as well as the parameters used – for A_T , equations are based on SSS only (Metzl et al., 1999; Shadwick et al., 2015) or using both SSS and SST (Lee et al., 2006; Laika et al., 2009) (Table 3). The highest bias and RSME are given by the equation of Shadwick et al. (2015) ($27.0 \pm 29.3 \mu\text{mol kg}^{-1}$). This can be explained by several factors: first, the equation is defined from SSS only for an area close to the STF. When using this equation for the entire transect through SAR and AAR, the dependence of A_T to changes in SST in the AAR is not considered, leading to important bias in the calculation of A_T . Moreover, the dataset used includes measurements over several seasons, while our dataset is restricted to the end of summer.

The other equations (Metzl et al., 1999; Lee et al., 2006; Laika et al., 2009) are in better agreement with the measured A_T . However, the error on the calculation of A_T using these formulas are still greater than when using Equ. 3. In detail, Lee et al. (2006) and Laika et al. (2009) equations are based on the relationship of A_T with SSS and SST. While Lee et al. (2006) equation is defined for the whole SO over all seasons, the equation used in Laika et al. (2009) is based on spring-summer measurements of year 2005–2006 along the same transect used in this study. Lee et al. (2006) calculated A_T present slightly lower error compared to Laika et al. (2009). Finally, Metzl et al. (1999) propose three equations using SSS only. The shifts and RMSE on the calculation of A_T are similar to the two previous formulas described when considering both SAR and AAR datasets together. However, when using Metzl et al. (1999) equations for SAR and AAR separately, the equations are a better fit in the SAR (mean shift of $4.4 \pm 8.4 \mu\text{mol kg}^{-1}$) than in the AAR ($15.2 \pm 16.6 \mu\text{mol kg}^{-1}$). This confirms the need to use SST in addition to SSS in the equation of A_T when considering the AAR.

The new equation developed in this study confirms a better fit with measured data compared to previously published equations, proving the

Table 2Coefficients of each term of the equation of $A_T = a + b \cdot \text{SSS} + c \cdot \text{SST}$ and $C_T = a + b \cdot \text{SSS} + c \cdot \text{SST} + d \cdot (\text{fCO}_{2\text{atm}} - 280)$.

	Region	a	b	c	d	Δ (measured – calculated)	RMSE	r^2
		(Intercept)	(SSS)	(SST)	($\text{fCO}_{2\text{atm}}$)			
A_T	SAR + AAR	762.69 ± 37.03	45.28 ± 1.11	-2.15 ± 0.10		-0.02	6.71	0.61
C_T	SAR	1431.45 ± 103.61	20.68 ± 3.22	-10.45 ± 0.50	0.56 ± 0.07	0.00	8.63	0.76
	AAR	-269.74 ± 256.1	70.42 ± 7.52	-6.27 ± 0.26	0.51 ± 0.06	0.25	8.15	0.62

Table 3Equation of A_T using physical parameters determined in the Southern Ocean.

Reference	Equation	ΔA_T ($\mu\text{mol kg}^{-1}$)	RMSE ($\mu\text{mol kg}^{-1}$)	Area	Period
Lee et al. (2006)	$A_T = 2305 + 52.48 \cdot (\text{SSS} - 35) + 2.85 \cdot (\text{SSS} - 35)^2 - 0.49 \cdot (\text{SST} - 20) + 0.086 \cdot (\text{SST} - 20)^2$	9.22	11.52	30°S – 60°S	All year
Shadwick et al. (2015)	$A_T = 53 \cdot \text{SSS} + 460$	26.96	29.31	46.8°S–142°E	Spring to Autumn
Laika et al. (2009)	$A_T = 434.711 - 2.599 \cdot \text{SST} + 54.671 \cdot \text{SSS}$	11.86	13.74	43°S–67°S and 140°E – 147°E	Spring–summer 2005/2006
Metzl et al. (1999)	$A_T = 37.58 \cdot \text{SSS} + 998.74$	11.88	14.73	South-West Indian Ocean (INDIGO-1)	March–April 1985
	$A_T = 35.978 \cdot \text{SSS} + 1055.9$	9.13	12.47	South-West Indian Ocean (INDIGO-3)	January–February 1987
	$A_T = 38.736 \cdot \text{SSS} + 960.5$	10.87	14.02	45°S–67°S and 140°E – 145°E (WOCE/SR3)	August 1996
This study	$A_T = 45.28 \cdot \text{SSS} - 2.15 \cdot \text{SST} + 762.69$	-0.01	6.71	43°S–67°S and 140°E – 147°E	Mid-February to Mid-march

interest of its use to complete the missing A_T values for long-term study of A_T variations during austral summer.

3.2.2. Drivers of C_T variability

As described earlier, C_T is linked to changes in SSS and SST in surface waters. It is also influenced by variations of biological activity, albeit to a lesser extent. Previous studies using empirical relationships to calculate C_T are often based on SSS, SST and a parameter related to biological activity such as Chl-a, Oxygen concentration or nutrients (Anderson and Sarmiento, 1994; Lee et al., 2000; Lo Monaco et al., 2005; Bates et al., 2006; Sarma et al., 2006; McNeil et al., 2007; Arrigo et al., 2010; Alin et al., 2012). However, for our study, no in situ measurements of nutrient or Chl-a are available. Moreover, satellite observations of Chl-a are 8-daily or monthly means and can be missing because of the important proportion of clouds in this region. The low-resolution Chl-a dataset compared to the rapid changes in biological activity in this area and to the high-resolution measurements of SST and SSS performed every minute could result in inaccuracy in the calculation of C_T . For these reasons, we do not use biological activity-related parameter to calculate C_T in this study. We are aware that the absence of biological activity-related parameter in the equation of C_T increases the error on the calculation, in particular when considering calculated C_T to estimate $\text{fCO}_{2\text{sw}}$. However, the spatial distribution of C_T is not firstly related to changes in biological activity, as seen when comparing the latitudinal variation in C_T and Chl-a (Fig. 3d and i), and using SSS and SST can help us retrieve the main C_T signal. Finally, this equation does not aim to help reconstruct $\text{fCO}_{2\text{sw}}$ data – that are often measured in-situ – but aims to better constrain C_T spatial and temporal variability in the SO based on well-measured physical parameters.

C_T is also dependent of atmospheric CO_2 concentration, including C_{ant} . Over the past decades, anthropogenic emissions have risen, leading to an increase in $\text{fCO}_{2\text{atm}}$ but also $\text{fCO}_{2\text{sw}}$ (Fig. 3f). This parameter is therefore important when dealing with the evolution of C_T through time. Lefèvre et al. (2021) included the year as a parameter to take into account the effect of atmospheric CO_2 evolution on C_T . Here we use $\text{fCO}_{2\text{atm}}$ instead as it resulted in reduced bias in C_T calculation compared to the year. While C_T is more directly related to changes in $\text{fCO}_{2\text{sw}}$ than $\text{fCO}_{2\text{atm}}$, the latter is measured at Cape Grim compared to $\text{fCO}_{2\text{sw}}$ that is calculated from A_T and C_T . This answers the willingness to develop an

equation that can be used with widespread parameters.

We developed a new simple equation for the calculation of C_T using SSS, SST and $\text{fCO}_{2\text{atm}}$. We use the term $(\text{fCO}_{2\text{atm}} - 280)$ in the equation to refer to the evolution of $\text{fCO}_{2\text{atm}}$ since the beginning of industrial period. Because the penetration of CO_2 in the ocean can be different in the SAR and AAR, we developed an equation for each region.

$$C_{T,\text{calc}} = a + b \cdot \text{SSS} + c \cdot \text{SST} + d \cdot (\text{fCO}_{2\text{atm}} - 280) \quad (4)$$

Coefficients are presented in Table 2. ΔC_T are $0.00 \pm 8.63 \mu\text{mol kg}^{-1}$ and $0.25 \pm 8.15 \mu\text{mol kg}^{-1}$ for SAR and AAR respectively. Because the few available equations allowing to calculate C_T in the surface SO use biological activity-related parameters or parameters that are not directly measured in our study (Lee et al., 2000; Laika et al., 2009), we could not compare our results with previous studies.

Using high resolution SST and SSS measured during the SURVOSTRAL cruises, when no in situ measurements of A_T and C_T are available, and using $\text{fCO}_{2\text{atm}}$ from Cape Grim station, A_T and C_T could be reconstructed during austral summer of all years from 2005 to 2019.

3.3. Interannual variability south of Tasmania from 2005 to 2019

Interannual and decadal evolution of the measured SST and SSS as well as A_T and C_T data over the period 2005–2019 are shown in Fig. 4 and Table 2 for the SAR and AAR. The trends are calculated using the mean value of February–March transects of each year.

3.3.1. Interannual variability in the SAR

In the SAR, SST and SSS both increased on average by $0.05 \pm 0.02 \text{ } ^\circ\text{C yr}^{-1}$ and $0.02 \pm 0.00 \text{ yr}^{-1}$ respectively (Table 4 and Fig. 4a and c). The surface waters south of Tasmania are influenced by the EAC, bringing salty and warm subtropical waters along the east coast of Tasmania. The volume of EAC flowing from the north depends on the wind stress curl. Over the past decades and in the context of global warming and climate change, an increase in wind stress curl have been observed in the Tasman Sea concomitant with a southward expansion of the subtropical gyre (Cai et al., 2005; Ridgway, 2007; Hill et al., 2008, 2011; Shears and Bowen, 2017), leading to a shift of the STF towards higher latitudes. No clear trend of STF shift was observed during austral summer (December

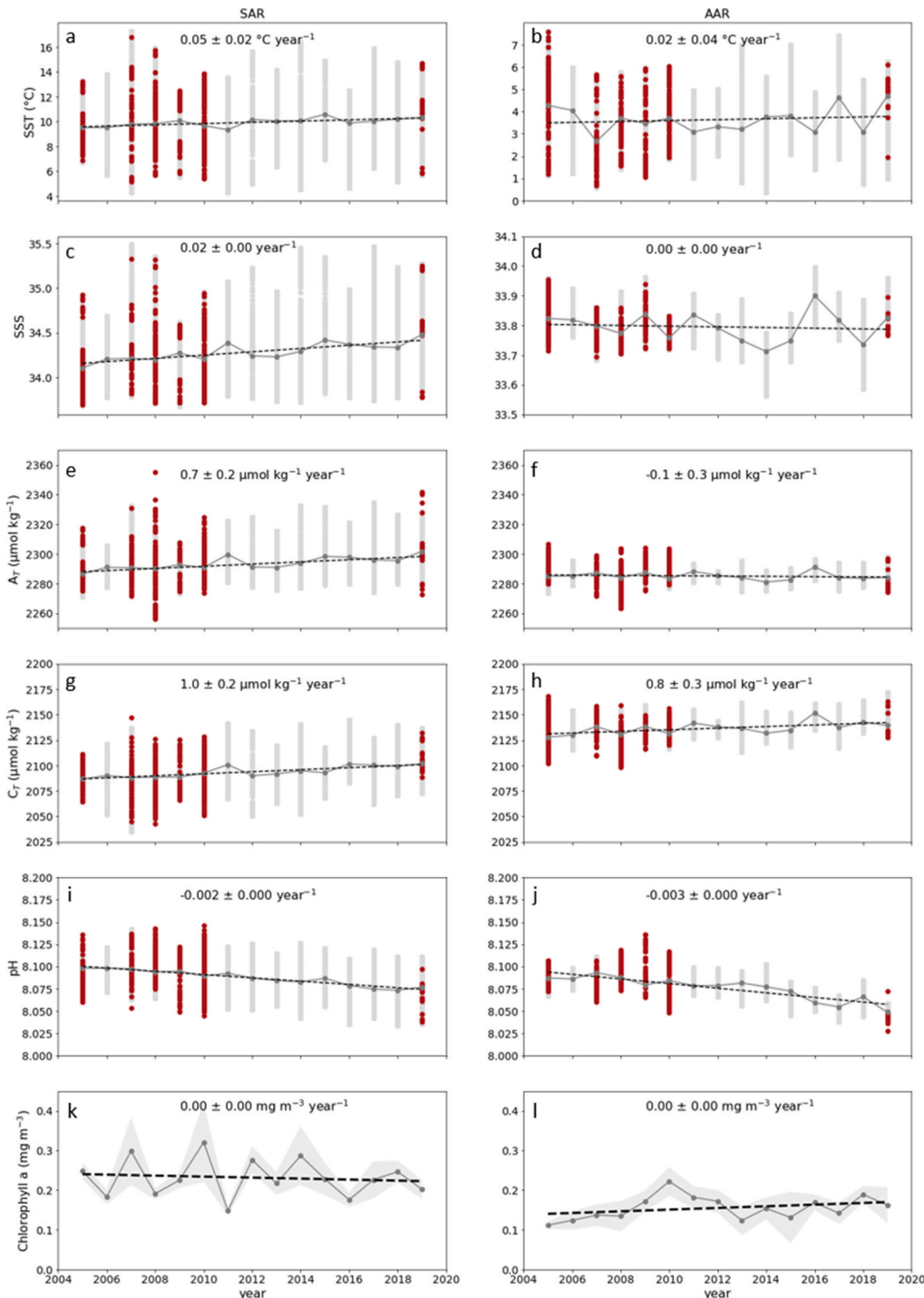


Fig. 4. Interannual variability of SST, SSS, A_T , C_T , pH and Chl-a from 2005 to 2019 for the SAR (a,c,e,g,i,k) and the AAR (b,d,f,h,j,l) using measured SST and SSS and calculated A_T and C_T from new equations developed in section 3.2 (light grey points are measured data of SST and SSS and calculated A_T and C_T . Dark grey points are yearly mean values and black dashed line is the linear regression of the mean values for each year as a function of time. Red points are data were measured A_T and C_T are available. For A_T and C_T trends, only calculated data were used.

to March) over the 1994–2012 period on the same transect using the 13 °C isotherm from TSG SST data to define the latitude of STF (Morrow and Kestenare, 2014). However, using both the strong gradient in SSS and the 13 °C isotherm on our dataset, the position of the STF at the surface seems to migrate southward during the period 2005–2019 (Supplementary Fig. 2). The increased inputs of warm and salty subtropical waters due to southward migration of the STF could explain the increase in SST and SSS in this region. Increase in SST and SSS in other part of the SO have also been observed in relation with the poleward shift of subtropical gyres and SO fronts (Gille, 2008; Sokolov and Rintoul, 2009; Armour et al., 2016; Sallée, 2018; Yang et al., 2020). A part of the warming observed in surface waters of the SAR south of Tasmania

could originate from the increasing heat uptake observed in the SO (Armour et al., 2016; Sallée, 2018; Auger et al., 2021). While some large-scale studies show a clear increase in SST in the region north of the PF in the SO, others present no clear trend, and similar observations have also been made for SSS (Midorikawa et al., 2012; Takahashi et al., 2014). However, the results may be difficult to compare depending on the period and area considered. Along the studied transect, the observed southward STF migration for the period 2005–2019 is smaller than the interannual variability. Moreover, the STF shows a strong mesoscale signature, with high variability of its position at the weekly scale, between two cruises the same year.

Reconstructed A_T increases by $0.7 \pm 0.2 \mu\text{mol kg}^{-1}\text{yr}^{-1}$ from 2005 to

Table 4

Decadal trends of SST, SSS, A_T and C_T observed in the SAR and AAR south of Tasmania over the period 2005–2019. The trend significance is computed using Python's module statsmodels with OLS regression model (Seabold and Perktold, 2010). r is the coefficient of correlation and p -value the probability of the null hypothesis, p -value = 0.001 indicating a 100% confidence level in the trend.

	Region	Slope	Error	r	p -value
SST ($^{\circ}\text{C yr}^{-1}$)	SAR	0.05	0.02	0.68	0.006
	AAR	0.02	0.04	0.15	0.58
SSS (yr^{-1})	SAR	0.02	0.00	0.82	<0.001
	AAR	0.00	0.00	-0.11	0.71
A_T ($\mu\text{mol kg}^{-1}\text{yr}^{-1}$)	SAR	0.7	0.2	0.77	<0.001
	AAR	-0.1	0.3	-0.17	0.18
C_T ($\mu\text{mol kg}^{-1}\text{yr}^{-1}$)	SAR	1.0	0.2	0.82	<0.001
	AAR	0.8	0.3	0.58	0.02
pH (yr^{-1})	SAR	-0.0018	0.0001	-0.89	<0.001
	AAR	-0.0026	0.0003	-0.96	<0.001
Chl-a ($\text{mg m}^{-3} \text{yr}^{-1}$)	SAR	0.00	0.00	-0.12	0.68
	AAR	0.00	0.00	0.32	0.25

2019 (Fig. 4e). While saltier waters tend to increase A_T , the increase in SST has the opposite effect. Using the coefficients of SST and SSS from A_T parametrization as well as the trends in SST and SSS in the SAR, we estimate the increase in A_T attributed to the rise in salinity to 0.91 ± 0.02 , while the effect of SST is only -0.11 ± 0.05 . The observed trend in A_T is therefore primarily impacted by the change in SSS due to increasing southward flow of subtropical waters through time. Long-term evolution of C_T presents an increase of $1.0 \pm 0.2 \mu\text{mol kg}^{-1} \text{yr}^{-1}$ (Fig. 4g). The C_T interannual trend is also influenced by the southward shift in subtropical waters. While the mean increase in SSS in the region also acts to increase C_T , the warming of surface waters reduces the CO_2 solubility, decreasing C_T . The $-0.53 \pm 0.24 \mu\text{mol kg}^{-1} \text{yr}^{-1}$ decrease in C_T linked to the $0.05 \pm 0.02 ^{\circ}\text{C yr}^{-1}$ increasing trend in SST in the SAR would be in part compensated by the $0.42 \pm 0.07 \mu\text{mol kg}^{-1} \text{yr}^{-1}$ rise due to the increasing trend in SSS. Moreover, biological activity variation can also affect the trend. In the SAR, interannual variability in Chl-a is observed, but the amplitude of this variability is small. No significant trend in the Chl-a concentration was observed during the period ($0.00 \pm 0.00 \text{ mg m}^{-3} \text{yr}^{-1}$, p -value = 0.68) (Fig. 4k), confirming that the observed trend in C_T is not influenced by biological activity over this period. Finally, C_T is also dependent on the variability of atmospheric CO_2 concentration and its exchange with surface waters. The increase in atmospheric CO_2 explains in part the rise in C_T . From 2005 to 2019, the $f\text{CO}_{2\text{atm}}$ increased at a rate of $2.1 \mu\text{atm yr}^{-1}$ at Cape Grim. Using the coefficient allocated to $f\text{CO}_{2\text{atm}}$ -280 in the equation of C_T , the estimated impact of $f\text{CO}_{2\text{atm}}$ variability on C_T trend is $1.18 \pm 0.15 \mu\text{mol kg}^{-1} \text{yr}^{-1}$. At the same time, pH decreases of $-0.0018 \pm 0.0001 \text{ yr}^{-1}$ in the SAR (Fig. 4i). These results, along with the observed increase in C_T , are consistent with the surface waters response to the rise in anthropogenic CO_2 uptake.

3.3.2. Interannual variability in the AAR

In the AAR, SST and SSS trends are not significant between 2005 and 2019 (Table 4), however they show interannual variability, with SST and SSS amplitudes varying by up to $2 ^{\circ}\text{C}$ and 0.2 respectively around the mean (Table 4 and Fig. 4b and d). The SO SST over the past decades presents different trends between north and south of the PF. North of the PF, surface waters are warming faster than South of the PF. In the South, SST increases more slowly in the Antarctic Zone, with a cooling in the sea-ice zone in eastern Antarctica (Armour et al., 2016; Sallée, 2018; Auger et al., 2021). The absence of significant change in SST in the entire AAR during the 2005–2019 period compared to the SAR, could be explained by this north-south difference. In the AAR, as defined in this study, late-summer surface waters are influenced by the advection of freshwater from regions of sea-ice melt and also high-salinity shelf waters at the southern end from sea-ice formation, both processes leading to a strong impact on SSS (Chaigneau et al., 2004). Indeed, Morrow and

Kestenare (2014) demonstrated that interannual variability in SSS was in part linked with sea-ice concentration, with years of higher sea-ice concentration in winter-spring leading to lower mean SSS the following summer, and vice versa.

As with SSS and SST, A_T shows no significant trend in the AAR (p -value = 0.93) (Fig. 4f) but presents interannual variability that is related to SSS and SST variability. In contrast, C_T presents a more robust trend, with a rate of $0.8 \pm 0.3 \mu\text{mol kg}^{-1} \text{yr}^{-1}$ through the period in the AAR (p -value = 0.02) (Fig. 4h). As in the SAR, Chl-a show no significant trend in the AAR (Fig. 4l). Therefore, we conclude that the biological activity has no impact on the long-term trend in C_T . However, we clearly see inter-annual variability in the biological activity. In particular, Chl-a shows a strong peak of 0.25 mg m^{-3} in 2010. In mid-February 2010, the calving of Mertz Glacier Tongue (Young et al., 2010) released multi-year, nutrient-rich sea-ice and led to increasing iron and light availability, consequently creating a diatom bloom in the area close to Antarctic Coast (Shadwick et al., 2013) and a higher biological activity in the area over the years after the event (Liniger et al., 2020). These findings could explain the slightly higher Chl-a concentration observed in the AAR after 2010 compared to the period before the calving event (Fig. 3). Because SST, SSS and Chl-a show no significant trend during the period 2005–2019, the increase in C_T is likely to originate from changes in air-sea exchanges of CO_2 . Using the same methodology as in the SAR, we estimate the influence of $f\text{CO}_{2\text{atm}}$ increase on C_T of $1.07 \pm 0.13 \mu\text{mol kg}^{-1} \text{yr}^{-1}$. Over the same period, we calculate a pH decrease of $-0.0026 \pm 0.0003 \text{ yr}^{-1}$ (Fig. 4j). As in the SAR, the pH trend agrees with the increase in C_T observed in this region.

3.3.3. Influence of anthropogenic carbon on C_T and pH

Estimates of long-term trends in C_T present an increase through time in all regions of the SO; with rates between 0.4 and $1.3 \mu\text{mol kg}^{-1} \text{yr}^{-1}$ (Midorikawa et al., 2012; Takahashi et al., 2014; Leseurre et al., 2022). These trends reflect the combined influence of changes in CO_2 solubility, biological activity, oceanic circulation and in the difference between atmospheric and surface-ocean $f\text{CO}_2$ (Carroll et al., 2022). Previous studies showed that the increase in C_T due to a $\sim 2 \mu\text{atm yr}^{-1}$ rise in atmospheric $p\text{CO}_2$ is around $1 \pm 0.2 \mu\text{mol kg}^{-1} \text{yr}^{-1}$ (Bates et al., 2002, 2012; Gruber et al., 2002; Lo Monaco et al., 2021). Using the coefficient associated with $f\text{CO}_{2\text{atm}}$ in the equation of C_T – and proposed here as to reflect the impact of the increase in anthropogenic carbon emissions on C_T , our estimates of $1.18 \pm 0.14 \mu\text{mol kg}^{-1} \text{yr}^{-1}$ and $1.07 \pm 0.13 \mu\text{mol kg}^{-1} \text{yr}^{-1}$ increase linked to $f\text{CO}_{2\text{atm}}$ trend in the SAR and AAR respectively are close to the expected trend. These estimates are subject to environmental uncertainty linked with the numerous mechanisms affecting C_T in surface waters, as described earlier. In order to increase the confidence on C_T trends and better understand the rate associated with anthropogenic emissions, observations on longer time periods are needed.

While the estimation of C_{ant} long-term evolution in surface waters is difficult, the impact of increasing C_T in surface waters on pH is unequivocal. In the SO, the rate of decrease in pH is estimated around $0.002 \pm 0.001 \text{ yr}^{-1}$ (Midorikawa et al., 2012; Takahashi et al., 2014; Munro et al., 2015; Lauvset et al., 2015; Williams et al., 2015; Xue et al., 2018; Leseurre et al., 2022). For the period 1969–2003 in the same study area, Midorikawa et al. (2012) found a more rapid pH decrease south of the PF ($-0.0020 \pm 0.0003 \text{ yr}^{-1}$) than in the Subantarctic Zone and Polar Front Zone (-0.0011 ± 0.0005 and $-0.0013 \pm 0.0004 \text{ yr}^{-1}$ respectively). More recently, in the western part of the Indian Southern Ocean, Leseurre et al. (2022) also show higher decreasing rates of pH south of the PF compared to the PFZ for observation sites that are not under the influence of Crozet and Kerguelen islands. We observe the same difference between the AAR and SAR in our study. As proposed by Midorikawa et al. (2012), while both regions are affected by the increase in C_{ant} in surface waters, the AAR is also subject to the upwelling of C_T -rich deep waters south of the PF. The slower decrease in pH estimated in the SAR compared to the AAR could also originate from the evolution of A_T

through time. While in the AAR, no significant changes in A_T are observed ($-0.1 \pm 0.3 \mu\text{mol kg}^{-1} \text{yr}^{-1}$), the rise in A_T in the SAR ($0.7 \pm 0.2 \mu\text{mol kg}^{-1} \text{yr}^{-1}$) could counteract in part the impact of increasing C_T on pH. The calculated rates of pH decrease for the period 2005–2019 in both the SAR and AAR in this study are higher than those observed for the period 1969–2003 (-0.0018 ± 0.0001 and $-0.0026 \pm 0.0003 \text{yr}^{-1}$ respectively). Similar observations have been made in the Mozambique Channel (Lo Monaco et al., 2021). This increase in the acidification rate is likely the result of the continuous increase in atmospheric CO_2 and is expected to further increase in the future (Jiang et al., 2019), with irreversible damages on ecosystems, in particular calcifying organisms (Doney et al., 2020).

4. Conclusion

The spatial and temporal variations in SST, SSS and the carbonate parameters have been explored using Mid-February to Mid-March data collected from 2005 to 2019 along a transect south of Tasmania. Latitudinal distribution of carbonate parameters reveals strong relationship with physical parameters. SST, SSS and A_T show high variability in the STZ and in the northern part of the SAR impacted by the strong meso-scale activity in these areas. In the CAZ, all parameters are influenced by the freshwater fluxes from sea-ice melting. CO_2 parameters show that the surface waters along the transect are a sink of CO_2 during summer, with a mean flux of $-4.0 \pm 2.8 \text{ mmol m}^{-2} \text{d}^{-1}$. The stronger sinks are located north of 51°S (in the STZ and northern part of the SAR) and south of 62°S , including the southern part of the AAR and the CAZ. They are associated with higher biological activity compared to the area between 51°S and 62°S . Relationships between physical and carbonate parameters are used in the SAR and AAR to determine new empirical relationship for the calculation of A_T and C_T , thus completing our dataset when no carbonate parameters are available. Using these equations, we calculated A_T and C_T for the period 2005–2019 in order to observe the decadal change in the surface biogeochemistry in both the SAR and AAR. In the SAR, the increase detected in SST and SSS has been linked to a southward migration of the Subtropical Front caused by the intensification of the wind stress curl and extension of the subtropical gyre north of the region. This change in hydrography also impacts A_T and C_T trends. C_T increases by $1.0 \pm 0.2 \mu\text{mol kg}^{-1} \text{yr}^{-1}$, which is attributed to the STF migration and to the increase in $f\text{CO}_{2\text{atm}}$. In the AAR, although SST, SSS and A_T show no significant trends, C_T increases by $0.8 \pm 0.3 \mu\text{mol kg}^{-1} \text{yr}^{-1}$. The sea-surface C_T increase caused by the rise in $f\text{CO}_{2\text{atm}}$ is estimated to be $1.18 \pm 0.14 \mu\text{mol kg}^{-1} \text{yr}^{-1}$ and $1.07 \pm 0.13 \mu\text{mol kg}^{-1} \text{yr}^{-1}$ in the SAR and AAR respectively. These estimates are close to the expected $1 \mu\text{mol kg}^{-1} \text{yr}^{-1}$ increase in C_T linked to the $+2.1 \text{ ppm yr}^{-1}$ of CO_2 recorded in the atmosphere during the period. Finally, the increase in C_T leads to an important decrease in pH (-0.0018 ± 0.0001 and $-0.0026 \pm 0.0003 \text{yr}^{-1}$ in the SAR and AAR respectively), implying a contribution towards ocean acidification processes and potential changes on the biogeochemistry of the ocean.

The A_T and C_T empirical relationships determined in this study, as well as the decadal evolution of physical and carbonate parameters in the SO bring new perspectives for the study of long-term evolution of the carbonate system. Monitoring of physical and biogeochemical parameters in the SO on regular and long-term basis are needed for a more complete study of the changes in ocean dynamics as well as carbonate and CO_2 systems from seasonal to decadal scales. Moreover, with the improvements of satellite observations of SST and SSS (Fine et al., 2017; Land et al., 2019), the calculation of A_T and C_T from empirical relationships could provide an even larger view of the carbonate system evolution in space and time.

Declaration of competing interest

The authors declare that they have no known competing financial interests or personal relationships that could have appeared to influence

the work reported in this paper.

Data availability

Data will be made available on request.

Acknowledgments

M. Brandon post-doctoral contract was funded by the European project ATLANTOS (grant agreement 633211). This work benefited from ICOS France project. The MINERVE program was supported by the French Institut Polaire Emile Victor (IPEV) as well as collaboration with Institut National des Sciences de l'Univers (INSU) and the CARbone AUstral Environmental Research Observatory (CARAUS). The SST and SSS data from the SURVOSTRAL program were obtained with the support of the IPEV, the ORE-SSS/LEGOS, and the CSIRO Marine and Atmospheric Research. We are grateful to Alain Poisson, who initiated the MINERVE program. We also thank Dmitry Khvorostyanov for useful discussions on data analysis. Analyses of Chl-a concentration from MODIS Aqua used in this study were downloaded from the Giovanni online data system, developed and maintained by the NASA Goddard Earth Sciences (GES) Data and Information Services Center (DISC).

Appendix A. Supplementary data

Supplementary data to this article can be found online at <https://doi.org/10.1016/j.dsr.2022.103836>.

References

- Alin, S.R., Feely, R.A., Dickson, A.G., Hernández-Ayón, J.M., Juranek, L.W., Ohman, M. D., Goericke, R., 2012. Robust empirical relationships for estimating the carbonate system in the southern California Current System and application to CalCOFI hydrographic cruise data (2005–2011). *J. Geophys. Res.* 117, C05033 <https://doi.org/10.1029/2011JC007511>.
- Alory, G., Delcroix, T., Téchéné, P., Diverres, D., Varillon, D., Cravatte, S., Gouriou, Y., Grelet, J., Jacquin, S., Kestenare, E., 2015. The French contribution to the voluntary observing ships network of sea surface salinity. *Deep Sea Res. Oceanogr. Res. Pap.* 105, 1–18. <https://doi.org/10.1016/j.dsr.2015.08.005>.
- Anderson, L.A., Sarmiento, J.L., 1994. Redfield ratios of remineralization determined by nutrient data analysis. *Global Biogeochem. Cycles* 8, 65–80. <https://doi.org/10.1029/93GB03318>.
- Armour, K.C., Marshall, J., Scott, J.R., Donohoe, A., Newsom, E.R., 2016. Southern Ocean warming delayed by circumpolar upwelling and equatorward transport. *Nat. Geosci.* 9, 549–554. <https://doi.org/10.1038/ngeo2731>.
- Arrigo, K.R., Pabi, S., van Dijken, G.L., Maslowski, W., 2010. air-sea flux of CO_2 in the Arctic ocean, 1998–2003. *J. Geophys. Res.* 115, G04024 <https://doi.org/10.1029/2009JG001224>.
- Auger, M., Morrow, R., Kestenare, E., Sallée, J.-B., Cowley, R., 2021. Southern Ocean in-situ temperature trends over 25 years emerge from interannual variability. *Nat. Commun.* 12, 514. <https://doi.org/10.1038/s41467-020-20781-1>.
- Bakker, D.C.E., Pfeil, B., Landa, C.S., Metzl, N., O'Brien, K.M., Olsen, A., Smith, K., Cosca, C., Harasawa, S., Jones, S.D., Nakaoka, S., Nojiri, Y., Schuster, U., Steinhoff, T., Sweeney, C., Takahashi, T., Tilbrook, B., Wada, C., Wanninkhof, R., Alin, S.R., Balestrini, C.F., Barbero, L., Bates, N.R., Bianchi, A.A., Bonou, F., Boutin, J., Bozec, Y., Burger, E.F., Cai, W.-J., Castle, R.D., Chen, L., Chierici, M., Currie, K., Evans, W., Featherstone, C., Feely, R.A., Fransson, A., Goyet, C., Greenwood, N., Gregor, L., Hankin, S., Hardman-Mountford, N.J., Harley, J., Hauck, J., Hoppema, M., Humphreys, M.P., Hunt, C.W., Huss, B., Ibáñez, J.S.P., Johannessen, T., Keeling, R., Kitidis, V., Körtzinger, A., Kozyr, A., Krasakopoulou, E., Kuwata, A., Landschützer, P., Lauvset, S.K., Lefèvre, N., Lo Monaco, C., Manke, A., Mathis, J.T., Merlivat, L., Millero, F.J., Monteiro, P.M.S., Munro, D.R., Murata, A., Newberger, T., Omar, A.M., Ono, T., Paterson, K., Pearce, D., Pierrot, D., Robbins, L. L., Saito, S., Salisbury, J., Schlitzer, R., Schneider, B., Schweitzer, R., Sieger, R., Skjelvan, I., Sullivan, K.F., Sutherland, S.C., Sutton, A.J., Tadokoro, K., Telszewski, M., Tuma, M., van Heuven, S.M.A.C., Vandemark, D., Ward, B., Watson, A.J., Xu, S., 2016. A multi-decade record of high-quality $f\text{CO}_2$: data in version 3 of the Surface Ocean CO_2 Atlas (SOCAT). *Earth Syst. Sci. Data* 8, 383–413. <https://doi.org/10.5194/essd-8-383-2016>.
- Balch, W.M., Bates, N.R., Lam, P.J., Twining, B.S., Rosengard, S.Z., Bowler, B.C., Drapeau, D.T., Garley, R., Lubelczyk, L.C., Mitchell, C., 2016. Factors regulating the great calcite belt in the Southern Ocean and its biogeochemical significance. *Global Biogeochem. Cycles* 30, 1124–1144. <https://doi.org/10.1002/2016GB005414>.
- Bates, N., Astor, Y., Church, M., Currie, K., Dore, J., Gonaález-Dávila, M., Lorenzoni, L., Muller-Karger, F., Olafsson, J., Santa-Casiano, M., 2014. A time-series view of changing ocean chemistry due to ocean uptake of anthropogenic CO_2 and ocean acidification. *oceanog* 27, 126–141. <https://doi.org/10.5670/oceanog.2014.16>.

- Bates, N.R., Best, M.H.P., Neely, K., Garley, R., Dickson, A.G., Johnson, R.J., 2012. Detecting anthropogenic carbon dioxide uptake and ocean acidification in the North Atlantic Ocean. *Biogeosciences* 9, 2509–2522. <https://doi.org/10.5194/bg-9-2509-2012>.
- Bates, N.R., Pequignet, A.C., Johnson, R.J., Gruber, N., 2002. A short-term sink for atmospheric CO₂ in subtropical mode water of the North Atlantic Ocean. *Nature* 420, 489–493. <https://doi.org/10.1038/nature01253>.
- Bates, N.R., Pequignet, A.C., Sabine, C.L., 2006. Ocean carbon cycling in the Indian Ocean: 1. Spatiotemporal variability of inorganic carbon and air-sea CO₂ gas exchange. *Global Biogeochem. Cycles* 20, GB3020. <https://doi.org/10.1029/2005GB002491>.
- Benallal, M.A., Moussa, H., Lencina-Avila, J.M., Touratier, F., Goyet, C., El Jai, M.C., Poisson, N., Poisson, A., 2017. Satellite-derived CO₂ flux in the surface seawater of the Austral Ocean south of Australia. *Int. J. Rem. Sens.* 38, 1600–1625. <https://doi.org/10.1080/01431161.2017.1286054>.
- Böning, C.W., Dispert, A., Visbeck, M., Rintoul, S.R., Schwarzkopf, F.U., 2008. The response of the Antarctic Circumpolar Current to recent climate change. *Nat. Geosci.* 1, 864–869. <https://doi.org/10.1038/ngeo362>.
- Brévière, E., Metzl, N., Poisson, A., Tilbrook, B., 2006. Changes of the oceanic CO₂ sink in the eastern Indian sector of the Southern Ocean. *Tellus B* 58, 438–446. <https://doi.org/10.1111/j.1600-0889.2006.00220.x>.
- Cai, W., Shi, G., Cowan, T., Bi, D., Ribbe, J., 2005. The response of the Southern Annular Mode, the East Australian Current, and the southern mid-latitude ocean circulation to global warming. *Geophys. Res. Lett.* 32, L23706 <https://doi.org/10.1029/2005GL024701>.
- Carroll, D., Menemenlis, D., Dutkiewicz, S., Lauderdale, J.M., Adkins, J.F., Bowman, K. W., Brix, H., Fenty, I., Gierach, M.E., Hill, C., Jahn, O., Landschützer, P., Manizza, M., Mazloff, M.R., Miller, F.J., Wijffels, S.E., Schimel, D.S., Verdy, A., Whitt, D.B., Zhang, H., 2022. Attribution of space-time variability in global-ocean dissolved inorganic carbon. *Global Biogeochem. Cycles* 36. <https://doi.org/10.1029/2021GB007162>.
- Carter, B.R., Feely, R.A., Wanninkhof, R., Kouketsu, S., Sonnerup, R.E., Pardo, P.C., Sabine, C.L., Johnson, G.C., Sloyan, B.M., Murata, A., Mecking, S., Tilbrook, B., Speer, K., Talley, L.D., Millero, F.J., Wijffels, S.E., Macdonald, A.M., Gruber, N., Bullister, J.L., 2019. Pacific anthropogenic carbon between 1991 and 2017. *Global Biogeochem. Cycles* 33, 597–617. <https://doi.org/10.1029/2018GB006154>.
- Chaigneau, A., Morrow, R., 2002. Surface temperature and salinity variations between Tasmania and Antarctica, 1993–1999. *J. Geophys. Res.* 107 <https://doi.org/10.1029/2001JC000808>. SRF 22-1-SRF 22-8.
- Chaigneau, A., Morrow, R.A., Rintoul, S.R., 2004. Seasonal and interannual evolution of the mixed layer in the Antarctic Zone south of Tasmania. *Deep Sea Res. Oceanogr. Res. Pap.* 51, 2047–2072. <https://doi.org/10.1016/j.dsr.2004.06.013>.
- Chen, C.T.A., 1993. The oceanic anthropogenic CO₂ sink. *Chemosphere* 27, 1041–1064. [https://doi.org/10.1016/0045-6535\(93\)90067-F](https://doi.org/10.1016/0045-6535(93)90067-F).
- Chen, C.T.A., 1982. On the distribution of anthropogenic CO₂ in the Atlantic and southern oceans. *Deep Sea Research Part A. Oceanogr. Res. Paper.* 29, 563–580. [https://doi.org/10.1016/0198-0149\(82\)90076-0](https://doi.org/10.1016/0198-0149(82)90076-0).
- Coatanoan, C., Goyet, C., Gruber, N., Sabine, C.L., Warner, M., 2001. Comparison of two approaches to quantify anthropogenic CO₂ in the ocean: results from the northern Indian Ocean. *Global Biogeochem. Cycles* 15, 11–25. <https://doi.org/10.1029/1999GB001200>.
- Cresswell, G., 2000. Currents of the continental shelf and upper slope of Tasmania. In: *Papers and Proceedings of the Royal Society of Tasmania*, pp. 21–30. <https://doi.org/10.26749/rstpp.133.3.21>.
- de Lavergne, C., Palter, J.B., Galbraith, E.D., Bernardello, R., Marinov, I., 2014. Cessation of deep convection in the open Southern Ocean under anthropogenic climate change. *Nat. Clim. Change* 4, 278–282. <https://doi.org/10.1038/nclimate2132>.
- DeVries, T., 2014. The oceanic anthropogenic CO₂ sink: storage, air-sea fluxes, and transports over the industrial era. *Global Biogeochem. Cycles* 28, 631–647. <https://doi.org/10.1002/2013GB004739>.
- Dickson, A.G., 1990. Standard potential of the reaction: AgCl (s) + 12H₂ (g) = Ag (s) + HCl (aq), and the standard acidity constant of the ion HSO₄⁻ in synthetic sea water from 273.15 to 318.15 K. *J. Chem. Therm.* 22, 113–127. [https://doi.org/10.1016/0021-9614\(90\)90074-Z](https://doi.org/10.1016/0021-9614(90)90074-Z).
- Dickson, A.G., Millero, F.J., 1987. A comparison of the equilibrium constants for the dissociation of carbonic acid in seawater media. *Deep Sea Research Part A. Oceanogr. Res. Paper.* 34, 1733–1743. [https://doi.org/10.1016/0198-0149\(87\)90021-5](https://doi.org/10.1016/0198-0149(87)90021-5).
- Doney, S.C., Busch, D.S., Cooley, S.R., Kroeker, K.J., 2020. The impacts of ocean acidification on marine ecosystems and reliant human communities. *Annu. Rev. Environ. Resour.* 45, 83–112. <https://doi.org/10.1146/annurev-environ-012320-083019>.
- Doney, S.C., Fabry, V.J., Feely, R.A., Kleypas, J.A., 2009. ocean acidification: the other CO₂ problem. *Annu. Rev. Mar. Sci.* 1, 169–192. <https://doi.org/10.1146/annurev.marine.010908.163834>.
- Durack, P.J., Wijffels, S.E., 2010. Fifty-year trends in global ocean salinities and their relationship to broad-scale warming. *J. Clim.* 23, 4342–4362. <https://doi.org/10.1175/2010JCLI3377.1>.
- Durack, P.J., Wijffels, S.E., Matear, R.J., 2012. Ocean salinities reveal strong global water cycle intensification during 1950 to 2000. *Science* 336, 455–458. <https://doi.org/10.1126/science.1212222>.
- Fine, R.A., Willey, D.A., Millero, F.J., 2017. Global variability and changes in ocean total alkalinity from Aquarius satellite data. *Geophys. Res. Lett.* 44, 261–267. <https://doi.org/10.1002/2016GL071712>.
- Friedlingstein, P., O'Sullivan, M., Jones, M.W., Andrew, R.M., Hauck, J., Olsen, A., Peters, G.P., Peters, W., Pongratz, J., Sitch, S., Le Quéré, C., Canadell, J.G., Ciais, P., Jackson, R.B., Alin, S., Aragão, L.E.O.C., Arneeth, A., Arora, V., Bates, N.R., Becker, M., Benoit-Cattin, A., Bittig, H.C., Bopp, L., Bultan, S., Chandra, N., Chevallier, F., Chini, L.P., Evans, W., Florentie, L., Forster, P.M., Gasser, T., Gehlen, M., Gilfillan, D., Gkritzalis, T., Gregor, L., Gruber, N., Harris, I., Hartung, K., Havard, V., Houghton, R.A., Ilyina, T., Jain, A.K., Joetzjer, E., Kadono, K., Kato, E., Kitidis, V., Korsbakken, J.L., Landschützer, P., Lefèvre, N., Lenton, A., Lienert, S., Liu, Z., Lombardo, D., Marland, G., Metzl, N., Munro, D.R., Nabel, J.E.M.S., Nakaoka, S.-I., Niwa, Y., O'Brien, K., Ono, T., Palmer, P.I., Pierrot, D., Poulter, B., Resplandy, L., Robertson, E., Rödenbeck, C., Schwinger, J., Séférian, R., Skjelvan, I., Smith, A.J.P., Sutton, A.J., Tanhua, T., Tans, P.P., Tian, H., Tilbrook, B., van der Werf, G., Vuichard, N., Walker, A.P., Wanninkhof, R., Watson, A.J., Willis, D., Wiltshire, A.J., Yuan, W., Yue, X., Zaehle, S., 2020. Global carbon budget 2020. *Earth Syst. Sci. Data* 12, 3269–3340. <https://doi.org/10.5194/essd-12-3269-2020>.
- Fry, C.H., Tyrrell, T., Hain, M.P., Bates, N.R., Achterberg, E.P., 2015. Analysis of global surface ocean alkalinity to determine controlling processes. *Mar. Chem.* 174, 46–57. <https://doi.org/10.1016/j.marchem.2015.05.003>.
- Garcia, H.E., Weathers, K.W., Paver, C.R., Smolyar, I., Boyer, T.P., Locarnini, M.M., Zweng, M.M., Mishonov, A.V., Baranova, O.K., Seidov, D., 2019. *World Ocean Atlas 2018. Vol. 4: dissolved inorganic nutrients (phosphate, nitrate and nitrate+ nitrite, silicate)*. NOAA Atlas NESDIS 84, 35pp.
- Gille, S.T., 2008. Decadal-scale temperature trends in the southern hemisphere ocean. *J. Clim.* 21, 4749–4765. <https://doi.org/10.1175/2008JCLI2131.1>.
- Goyet, C., Beauverger, C., Brunet, C., Poisson, A., 1991. Distribution of carbon dioxide partial pressure in surface waters of the Southwest Indian Ocean. *Tellus B* 43, 1–11. <https://doi.org/10.1034/j.1600-0889.1991.00001.x>.
- Gray, A.R., Johnson, K.S., Bushinsky, S.M., Riser, S.C., Russell, J.L., Talley, L.D., Wanninkhof, R., Williams, N.L., Sarmiento, J.L., 2018. Autonomous biogeochemical floats detect significant carbon dioxide outgassing in the high-latitude Southern Ocean. *Geophys. Res. Lett.* 45, 9049–9057. <https://doi.org/10.1029/2018GL078013>.
- Gregor, Luke, Gruber, Nicolas, 2021. OceanSODA-ETHZ: a global gridded data set of the surface ocean carbonate system for seasonal to decadal studies of ocean acidification. *Earth Syst. Sci. Data* 13, 777–808. <https://doi.org/10.5194/essd-13-777-2021>.
- Gruber, N., Clement, D., Carter, B.R., Feely, R.A., van Heuven, S., Hoppema, M., Ishii, M., Key, R.M., Kozyr, A., Lauvset, S.K., Lo Monaco, C., Mathis, J.T., Murata, A., Olsen, A., Perez, F.F., Sabine, C.L., Tanhua, T., Wanninkhof, R., 2019a. The oceanic sink for anthropogenic CO₂ from 1994 to 2007. *Science* 363, 1193–1199. <https://doi.org/10.1126/science.aau5153>.
- Gruber, N., Gloor, M., Mikaloff Fletcher, S.E., Doney, S.C., Dutkiewicz, S., Follows, M.J., Gerber, M., Jacobson, A.R., Joos, F., Lindsay, K., Menemenlis, D., Mouchet, A., Müller, S.A., Sarmiento, J.L., Takahashi, T., 2009. Oceanic sources, sinks, and transport of atmospheric CO₂. *Global Biogeochem. Cycles* 23, GB1005. <https://doi.org/10.1029/2008GB003349>.
- Gruber, N., Keeling, C.D., Bates, N.R., 2002. Interannual variability in the north Atlantic ocean carbon sink. *Science* 298, 2374–2378. <https://doi.org/10.1126/science.1077077>.
- Gruber, N., Landschützer, P., Lovenduski, N.S., 2019b. The variable Southern Ocean carbon sink. *Ann. Rev. Mar. Sci.* 11, 159–186. <https://doi.org/10.1146/annurev-marine-121916-063407>.
- Haumann, F.A., Gruber, N., Münnich, M., Frenger, I., Kern, S., 2016. Sea-ice transport driving Southern Ocean salinity and its recent trends. *Nature* 537, 89–92. <https://doi.org/10.1038/nature19101>.
- Herraz-Borreguero, L., Rintoul, S.R., 2011. Regional circulation and its impact on upper ocean variability south of Tasmania. *Deep Sea Res. Part II Top. Stud. Oceanogr.* 58, 2071–2081. <https://doi.org/10.1016/j.dsr2.2011.05.022>.
- Herraz-Borreguero, L., Rintoul, S.R., 2010. Subantarctic Mode Water variability influenced by mesoscale eddies south of Tasmania. *J. Geophys. Res.: Oceans* 115. <https://doi.org/10.1029/2008JC005146>.
- Hill, K.L., Rintoul, S.R., Coleman, R., Ridgway, K.R., 2008. Wind forced low frequency variability of the East Australia Current. *Geophys. Res. Lett.* 35, L08602 <https://doi.org/10.1029/2007GL032912>.
- Hill, K.L., Rintoul, S.R., Ridgway, K.R., Oke, P.R., 2011. Decadal changes in the South Pacific western boundary current system revealed in observations and ocean state estimates. *J. Geophys. Res.* 116, C01009 <https://doi.org/10.1029/2009JC005926>.
- Humphreys, M.P., Schiller, A.J., Sandborn, D.E., Gregor, L., Pierrot, D., van Heuven, S.M. A.C., Lewis, E.R., Wallace, D.W.R., 2022. PyCO2SYS: marine carbonate system calculations in Python. *Zenodo*. <https://doi.org/10.5281/zenodo.3744275>.
- Jiang, L.-Q., Carter, B.R., Feely, R.A., Lauvset, S.K., Olsen, A., 2019. Surface ocean pH and buffer capacity: past, present and future. *Sci. Rep.* 9, 18624 <https://doi.org/10.1038/s41598-019-55039-4>.
- Key, R.M., Kozyr, A., Sabine, C.L., Lee, K., Wanninkhof, R., Bullister, J.L., Feely, R.A., Millero, F.J., Mordy, C., Peng, T.-H., 2004. A global ocean carbon climatology: results from global data analysis project (GLODAP). *Global Biogeochem. Cycles* 18, GB4031. <https://doi.org/10.1029/2004GB002247>.
- Laika, H.E., Goyet, C., Vouve, F., Poisson, A., Touratier, F., 2009. Interannual properties of the CO₂ system in the Southern Ocean south of Australia. *Antarct. Sci.* 21, 663–680. <https://doi.org/10.1017/S0954102009990319>.
- Land, P.E., Findlay, H.S., Shutler, J.D., Ashton, I.G.C., Holding, T., Grouazel, A., Girard-Audhuin, F., Reul, N., Piolle, J.-F., Chapron, B., Quillen, Y., Bellerby, R.G.J., Bhadury, P., Salisbury, J., Vandemark, D., Sabia, R., 2019. Optimum satellite remote sensing of the marine carbonate system using empirical algorithms in the global ocean, the Greater Caribbean, the Amazon Plume and the Bay of Bengal. *Rem. Sens. Environ.* 235, 111469 <https://doi.org/10.1016/j.rse.2019.111469>.
- Landschützer, P., Gruber, N., Haumann, F.A., Rödenbeck, C., Bakker, D.C.E., van Heuven, S., Hoppema, M., Metzl, N., Sweeney, C., Takahashi, T., Tilbrook, B.,

- Wanninkhof, R., 2015. The reinvigoration of the Southern Ocean carbon sink. *Science* 349, 1221–1224. <https://doi.org/10.1126/science.aab2620>.
- Lausvset, S.K., Gruber, N., Landschützer, P., Olsen, A., Tjiputra, J., 2015. Trends and drivers in global surface ocean pH over the past 3 decades. *Biogeosciences* 12, 1285–1298. <https://doi.org/10.5194/bg-12-1285-2015>.
- Le Quéré, C., Rödenbeck, C., Buitenhuis, E.T., Conway, T.J., Langenfelds, R., Gomez, A., Labuschagne, C., Ramonet, M., Nakazawa, T., Metzl, N., Gillett, N., Heimann, M., 2007. Saturation of the Southern Ocean CO₂ sink due to recent climate change. *Science* 316, 1735–1738. <https://doi.org/10.1126/science.1136188>.
- Lee, K., Tong, L.T., Millero, F.J., Sabine, C.L., Dickson, A.G., Goyet, C., Park, G.-H., Wanninkhof, R., Feely, R.A., Key, R.M., 2006. Global relationships of total alkalinity with salinity and temperature in surface waters of the world's oceans. *Geophys. Res. Lett.* 33, L19605. <https://doi.org/10.1029/2006GL027207>.
- Lee, K., Wanninkhof, R., Feely, R.A., Millero, F.J., Peng, T.-H., 2000. Global relationships of total inorganic carbon with temperature and nitrate in surface seawater. *Global Biogeochem. Cycles* 14, 979–994. <https://doi.org/10.1029/1998GB001087>.
- Lefèvre, N., Mejia, C., Khvorostyanov, D., Beaumont, L., Koffi, U., 2021. Ocean circulation drives the variability of the carbon system in the eastern tropical Atlantic. *Oceans* 2, 126–148. <https://doi.org/10.3390/oceans2010008>.
- Lenton, A., Metzl, N., Takahashi, T., Kuchinke, M., Matear, R.J., Roy, T., Sutherland, S.C., Sweeney, C., Tilbrook, B., 2012. The observed evolution of oceanic pCO₂ and its drivers over the last two decades. *Global Biogeochem. Cycles* 26, GB2021. <https://doi.org/10.1029/2011GB004095>.
- Lenton, A., Tilbrook, B., Law, R.M., Bakker, D., Doney, S.C., Gruber, N., Ishii, M., Hoppema, M., Lovenduski, N.S., Matear, R.J., McNeil, B.I., Metzl, N., Mikaloff Fletcher, S.E., Monteiro, P.M.S., Rödenbeck, C., Sweeney, C., Takahashi, T., 2013. Sea-air CO₂ fluxes in the Southern Ocean for the period 1990–2009. *Biogeosciences* 10, 4037–4054. <https://doi.org/10.5194/bg-10-4037-2013>.
- Leseurre, C., Lo Monaco, C., Reverdin, G., Metzl, N., Fin, J., Mignon, C., Benito, L., 2022. Summer trends and drivers of sea surface fCO₂ and pH changes observed in the Southern Indian Ocean over the last two decades (1998–2019). *Biogeosciences* 19, 2599–2625. <https://doi.org/10.5194/bg-19-2599-2022>.
- Lewis, E.R., Wallace, D.W.R., 1998. Program Developed for CO₂ System Calculations. Environmental System Science Data Infrastructure for a Virtual Ecosystem, United States.
- Liniger, G., Strutton, P.G., Lannuzel, D., Moreau, S., 2020. Calving event led to changes in phytoplankton bloom phenology in the Mertz polynya, Antarctica. *J. Geophys. Res.: Oceans* 125, e2020JC016387. <https://doi.org/10.1029/2020JC016387>.
- Lo Monaco, C., Goyet, C., Metzl, N., Poisson, A., Touratier, F., 2005. Distribution and inventory of anthropogenic CO₂ in the Southern Ocean: comparison of three data-based methods. *J. Geophys. Res.* 110. <https://doi.org/10.1029/2004JC002571>.
- Lo Monaco, C., Metzl, N., Fin, J., Mignon, C., Cuet, P., Douville, E., Gehlen, M., Chau, T.T., Tribollet, A., 2021. Distribution and long-term change of the sea surface carbonate system in the Mozambique Channel (1963–2019). In: *Deep Sea Research Part II: Topical Studies in Oceanography* 186–188, 104936. <https://doi.org/10.1016/j.dsr2.2021.104936>.
- Lourantou, A., Metzl, N., 2011. Decadal evolution of carbon sink within a strong bloom area in the subantarctic zone. *Geophys. Res. Lett.* 38, L23608. <https://doi.org/10.1029/2011GL049614>.
- Lovenduski, N.S., Gruber, N., Doney, S.C., 2008. Toward a mechanistic understanding of the decadal trends in the Southern Ocean carbon sink. *Global Biogeochem. Cycles* 22, GB3016. <https://doi.org/10.1029/2007GB003139>.
- Mahieu, L., Lo Monaco, C., Metzl, N., Fin, J., Mignon, C., 2020. Variability and stability of anthropogenic CO₂ in Antarctic bottom water observed in the Indian sector of the Southern Ocean. *Ocean Sci.* 16, 1559–1576. <https://doi.org/10.5194/os-16-1559-2020>.
- McNeil, B.I., Metzl, N., Key, R.M., Matear, R.J., Corbiere, A., 2007. An empirical estimate of the Southern Ocean air-sea CO₂ flux. *Global Biogeochem. Cycles* 21, GB3011. <https://doi.org/10.1029/2007GB002991>.
- Mehrbach, C., Culbertson, C.H., Hawley, J.E., Pytkowicz, R.M., 1973. Measurement of the apparent dissociation constants of carbonic acid in seawater at atmospheric pressure 1. *Limnol. Oceanogr.* 18, 897–907. <https://doi.org/10.4319/l.1973.18.6.0897>.
- Merlivat, L., Boutin, J., Antoine, D., Beaumont, L., Golbol, M., Vellucci, V., 2018. Increase of dissolved inorganic carbon and decrease in pH in near-surface waters in the Mediterranean Sea during the past two decades. *Biogeosciences* 15, 5653–5662. <https://doi.org/10.5194/bg-15-5653-2018>.
- Metzl, N., 2009. Decadal increase of oceanic carbon dioxide in Southern Indian Ocean surface waters (1991–2007). *Deep Sea Res. Part II Top. Stud. Oceanogr.* 56, 607–619. <https://doi.org/10.1016/j.dsr2.2008.12.007>.
- Metzl, N., Brunet, C., Jabaud-Jan, A., Poisson, A., Schauer, B., 2006. Summer and winter air-sea CO₂ fluxes in the Southern Ocean. *Deep Sea Res. Oceanogr. Res. Pap.* 53, 1548–1563. <https://doi.org/10.1016/j.dsr.2006.07.006>.
- Metzl, N., Lo Monaco, C., Leseurre, C., Ridame, C., Fin, J., Mignon, C., Gehlen, M., Chau, T.T.T., 2022. The impact of the South-East Madagascar Bloom on the oceanic CO₂ sink. *Biogeosciences* 19, 1451–1468. <https://doi.org/10.5194/bg-19-1451-2022>.
- Metzl, N., Poisson, A., Louanchi, F., Brunet, C., Schauer, B., Bres, B., 1995. Spatio-temporal distributions of air-sea fluxes of CO₂ in the Indian and Antarctic oceans. *Tellus B* 47, 56–69. <https://doi.org/10.3402/tellusb.v47i1-2.16006>.
- Metzl, N., Tilbrook, B., Poisson, A., 1999. The annual CO₂ cycle and the air-sea CO₂ flux in the sub-Antarctic Ocean. *Tellus B* 51, 849–861. <https://doi.org/10.1034/j.1600-0889.1999.t013-0-00008.x>.
- Midorikawa, T., Inoue, H.Y., Ishii, M., Sasano, D., Kosugi, N., Hashida, G., Nakaoka, S., Suzuki, T., 2012. Decreasing pH trend estimated from 35-year time series of carbonate parameters in the Pacific sector of the Southern Ocean in summer. *Deep Sea Res. Oceanogr. Res. Pap.* 61, 131–139. <https://doi.org/10.1016/j.dsr.2011.12.003>.
- Mikaloff Fletcher, S.E., Gruber, N., Jacobson, A.R., Doney, S.C., Dutkiewicz, S., Gerber, M., Follows, M., Joos, F., Lindsay, K., Menemenlis, D., Mouchet, A., Müller, S.A., Sarmiento, J.L., 2006. Inverse estimates of anthropogenic CO₂ uptake, transport, and storage by the ocean. *Global Biogeochem. Cycles* 20, GB2002. <https://doi.org/10.1029/2005GB002530>.
- Millero, F.J., Lee, K., Roche, M., 1998. Distribution of alkalinity in the surface waters of the major oceans. *Mar. Chem.* 60, 111–130. [https://doi.org/10.1016/S0304-4203\(97\)00084-4](https://doi.org/10.1016/S0304-4203(97)00084-4).
- Moreau, S., Penna, A.D., Llort, J., Patel, R., Langlais, C., Boyd, P.W., Matear, R.J., Phillips, H.E., Trull, T.W., Tilbrook, B., Lenton, A., Strutton, P.G., 2017. Eddy-induced carbon transport across the Antarctic circumpolar current: eddy-induced carbon transport. *Global Biogeochem. Cycles* 31, 1368–1386. <https://doi.org/10.1002/2017GB005669>.
- Morrow, R., Donguy, J.-R., Chaigneau, A., Rintoul, S.R., 2004. Cold-core anomalies at the subantarctic front, south of Tasmania. *Deep Sea Res. Oceanogr. Res. Pap.* 51, 1417–1440. <https://doi.org/10.1016/j.dsr.2004.07.005>.
- Morrow, R., Kestenare, E., 2017. 22-year surface salinity changes in the Seasonal Ice Zone near 140°E off Antarctica. *J. Mar. Syst.* 175, 46–62. <https://doi.org/10.1016/j.jmarsys.2017.07.003>.
- Morrow, R., Kestenare, E., 2014. Nineteen-year changes in surface salinity in the Southern Ocean south of Australia. *J. Mar. Syst.* 129, 472–483. <https://doi.org/10.1016/j.jmarsys.2013.09.011>.
- Munro, D.R., Lovenduski, N.S., Takahashi, T., Stephens, B.B., Newberger, T., Sweeney, C., 2015. Recent evidence for a strengthening CO₂ sink in the Southern Ocean from carbonate system measurements in the Drake Passage (2002–2015). *Geophys. Res. Lett.* 42, 7623–7630. <https://doi.org/10.1002/2015GL065194>.
- Murata, A., Kumamoto, Y., Sasaki, K., Watanabe, S., Fukasawa, M., 2010. Decadal increases in anthropogenic CO₂ along 20°S in the south Indian ocean. *J. Geophys. Res.* 115, C12055. <https://doi.org/10.1029/2010JC006250>.
- Nissen, C., Gruber, N., Münnich, M., Vogt, M., 2021. Southern Ocean phytoplankton community structure as a gatekeeper for global nutrient biogeochemistry. *Global Biogeochem. Cycles* 35. <https://doi.org/10.1029/2021GB006991>.
- Oliver, E.C.J., Herzfeld, M., Holbrook, N.J., 2016. Modelling the shelf circulation off eastern Tasmania. *Contin. Shelf Res.* 130, 14–33. <https://doi.org/10.1016/j.csr.2016.10.005>.
- Oliver, E.C.J., Holbrook, N.J., 2018. Variability and long-term trends in the shelf circulation off eastern Tasmania. *J. Geophys. Res. Oceans* 123, 7366–7381. <https://doi.org/10.1029/2018JC013994>.
- Orr, J.C., Fabry, V.J., Aumont, O., Bopp, L., Doney, S.C., Feely, R.A., Gnanadesikan, A., Gruber, N., Ishida, A., Joos, F., Key, R.M., Lindsay, K., Maier-Reimer, E., Matear, R., Monfray, P., Mouchet, A., Najjar, R.G., Plattner, G.-K., Rodgers, K.B., Sabine, C.L., Sarmiento, J.L., Schlitzer, R., Slater, R.D., Totterdell, I.J., Weirig, M.-F., Yamanaka, Y., Yool, A., 2005. Anthropogenic ocean acidification over the twenty-first century and its impact on calcifying organisms. *Nature* 437, 681–686. <https://doi.org/10.1038/nature04095>.
- Orsi, A.H., Whitworth III, T., Nowlin Jr., W.D., 1995. On the meridional extent and fronts of the Antarctic Circumpolar Current. *Deep Sea Res. Oceanogr. Res. Pap.* 42, 641–673. [https://doi.org/10.1016/0967-0637\(95\)00021-W](https://doi.org/10.1016/0967-0637(95)00021-W).
- Pardo, P.C., Tilbrook, B., Langlais, C., Trull, T.W., Rintoul, S.R., 2017. Carbon uptake and biogeochemical change in the Southern Ocean, south of Tasmania. *Biogeosciences* 14, 5217–5237. <https://doi.org/10.5194/bg-14-5217-2017>.
- Park, Y.-H., Park, T., Kim, T.-W., Lee, S.-H., Hong, C.-S., Lee, J.-H., Rio, M.-H., Pujol, M.-I., Ballarotta, M., Durand, I., Provost, C., 2019. Observations of the Antarctic circumpolar current over the uidintsev fracture zone, the narrowest choke point in the Southern Ocean. *J. Geophys. Res. Oceans* 124, 4511–4528. <https://doi.org/10.1029/2019JC015024>.
- Peng, T.-H., Wanninkhof, R., 2010. Increase in anthropogenic CO₂ in the Atlantic Ocean in the last two decades. *Deep Sea Res. Oceanogr. Res. Pap.* 57, 755–770. <https://doi.org/10.1016/j.dsr.2010.03.008>.
- Ridgway, K.R., 2007. Long-term trend and decadal variability of the southward penetration of the East Australian Current. *Geophys. Res. Lett.* 34, L13613. <https://doi.org/10.1029/2007GL030393>.
- Sabine, C.L., Feely, R.A., Gruber, N., Key, R.M., Lee, K., Bullister, J.L., Wanninkhof, R., Wong, C.S., Wallace, D.W.R., Tilbrook, B., Millero, F.J., Peng, T.-H., Kozyr, A., Ono, T., Rios, A.F., 2004. The oceanic sink for anthropogenic CO₂. *Science* 305, 367–371. <https://doi.org/10.1126/science.1097403>.
- Sabine, C.L., Tanhua, T., 2010. Estimation of anthropogenic CO₂ inventories in the ocean. *Ann. Rev. Mar. Sci.* 2, 175–198. <https://doi.org/10.1146/annurev-marine-120308-080947>.
- Sallée, J.-B., 2018. Southern Ocean warming. *Oceanography* 31. <https://doi.org/10.5670/oceanog.2018.215>.
- Sarma, V.V.S.S., Saino, T., Sasaoka, K., Nojiri, Y., Ono, T., Ishii, M., Inoue, H.Y., Matsumoto, K., 2006. Basin-scale pCO₂ distribution using satellite sea surface temperature, Chl *a*, and climatological salinity in the North Pacific in spring and summer. *Global Biogeochem. Cycles* 20, GB3005. <https://doi.org/10.1029/2005GB002594>.
- Seabold, S., Perktold, J., 2010. Statsmodels: econometric and statistical modeling with python. In: *Proceedings of the 9th Python in Science Conference*, pp. 57–61. Austin, TX.
- Shadwick, E.H., Rintoul, S.R., Tilbrook, B., Williams, G.D., Young, N., Fraser, A.D., Marchant, H., Smith, J., Tamura, T., 2013. Glacier tongue calving reduced dense water formation and enhanced carbon uptake. *Geophys. Res. Lett.* 40, 904–909. <https://doi.org/10.1002/grl.50178>.

- Shadwick, E.H., Trull, T.W., Tilbrook, B., Sutton, A.J., Schulz, E., Sabine, C.L., 2015. Seasonality of biological and physical controls on surface ocean CO₂ from hourly observations at the Southern Ocean Time Series site south of Australia. *Global Biogeochem. Cycles* 29, 223–238. <https://doi.org/10.1002/2014GB004906>.
- Shears, N.T., Bowen, M.M., 2017. Half a century of coastal temperature records reveal complex warming trends in western boundary currents. *Sci. Rep.* 7, 14527 <https://doi.org/10.1038/s41598-017-14944-2>.
- Sokolov, S., Rintoul, S.R., 2009. Circumpolar structure and distribution of the Antarctic Circumpolar Current fronts: 2. Variability and relationship to sea surface height. *J. Geophys. Res.* 114, C11019 <https://doi.org/10.1029/2008JC005248>.
- Sokolov, S., Rintoul, S.R., 2002. Structure of Southern Ocean fronts at 140°E. *J. Mar. Syst.* 34 [https://doi.org/10.1016/S0924-7963\(02\)00200-2](https://doi.org/10.1016/S0924-7963(02)00200-2).
- Takahashi, T., Sutherland, S.C., Chipman, D.W., Goddard, J.G., Ho, C., Newberger, T., Sweeney, C., Munro, D.R., 2014. Climatological distributions of pH, pCO₂, total CO₂, alkalinity, and CaCO₃ saturation in the global surface ocean, and temporal changes at selected locations. *Mar. Chem.* 164, 95–125. <https://doi.org/10.1016/j.marchem.2014.06.004>.
- Takahashi, T., Sutherland, S.C., Wanninkhof, R., Sweeney, C., Feely, R.A., Chipman, D.W., Hales, B., Friederich, G., Chavez, F., Sabine, C., Watson, A., Bakker, D.C.E., Schuster, U., Metzl, N., Yoshikawa-Inoue, H., Ishii, M., Midorikawa, T., Nojiri, Y., Körtzinger, A., Steinhoff, T., Hoppema, M., Olafsson, J., Arnarson, T.S., Tilbrook, B., Johannessen, T., Olsen, A., Bellerby, R., Wong, C.S., Delille, B., Bates, N.R., de Baar, H.J.W., 2009. Climatological mean and decadal change in surface ocean pCO₂, and net sea–air CO₂ flux over the global oceans. *Deep Sea Res. Part II Top. Stud. Oceanogr.* 56, 554–577. <https://doi.org/10.1016/j.dsr2.2008.12.009>.
- Wanninkhof, R., 2014. Relationship between wind speed and gas exchange over the ocean revisited: gas exchange and wind speed over the ocean. *Limnol. Oceanogr. Methods* 12, 351–362. <https://doi.org/10.4319/lom.2014.12.351>.
- Weiss, R.F., 1974. CO₂ in water and seawater: the solubility of a non-ideal gas. *Mar. Chem.* 2 (3), 203–215.
- Wentz, F.J., Scott, J., Hoffman, R., Leidner, M., Atlas, R., Ardizzone, J., 2015. Remote Sensing Systems Cross-Calibrated Multi-Platform (CCMP) 6-hourly Ocean Vector Wind Analysis Product on 0.25 Deg Grid, Version 2.0. Remote Sensing Systems, Santa Rosa, CA.
- Williams, N.L., Feely, R.A., Sabine, C.L., Dickson, A.G., Swift, J.H., Talley, L.D., Russell, J.L., 2015. Quantifying anthropogenic carbon inventory changes in the Pacific sector of the Southern Ocean. *Mar. Chem.* 174, 147–160. <https://doi.org/10.1016/j.marchem.2015.06.015>.
- Wu, Y., Hain, M.P., Humphreys, M.P., Hartman, S., Tyrrell, T., 2019. What drives the latitudinal gradient in open-ocean surface dissolved inorganic carbon concentration? *Biogeosciences* 16, 2661–2681. <https://doi.org/10.5194/bg-16-2661-2019>.
- Xue, L., Cai, W.-J., Takahashi, T., Gao, L., Wanninkhof, R., Wei, M., Li, K., Feng, L., Yu, W., 2018. Climatic modulation of surface acidification rates through summertime wind forcing in the Southern Ocean. *Nat. Commun.* 9, 3240. <https://doi.org/10.1038/s41467-018-05443-7>.
- Yang, H., Lohmann, G., Krebs-Kanzow, U., Ionita, M., Shi, X., Sidorenko, D., Gong, X., Chen, X., Gowan, E.J., 2020. Poleward shift of the major ocean gyres detected in a warming climate. *Geophys. Res. Lett.* 47 <https://doi.org/10.1029/2019GL085868>.
- Young, N., Legresy, B., Coleman, R., Massom, R., 2010. Mertz Glacier tongue unhinged by giant iceberg. *Aust. Antarct. Mag.* 18, 19.